The *Nkx2.3–Nr5a1* gene cascade plays a crucial role in spleen-specific vascular architecture and marginal zone formation

Kanako Miyabayashi[1*], Koji Ono[2*†], Tetsuya Sato[3], Ayano Yahagi[4§], Masanori Iseki[4], Katsuhiko Ishihara[4¶], Takami Mori[5‡], Miki Inoue[1], Ryuki Shimada[6], Kei-ichiro Ishiguro[7], Tomohiro Ishii[8], Jongsung Noh[9], Man Ho Choi[9], Takashi Baba[10], Yasuyuki Ohkawa[11], Emi Kiyokage[5], Kazunori Toida[2], Yuichi Shima[1]

[1]Division of Microscopic and Developmetal Anatomy, Department of Anatomy, Kurume University, School of Medicine, 67 Asahi-machi, Kurume, Fukuoka 830-0011, Japan

[2]Department of Anatomy, Kawasaki Medical School, 577 Matsushima, Kurashiki, Okayama 701-0192, Japan

[3]Biomedical Research Center, Faculty of Medicine, Saitama Medical University, 1397-1 Yamane, Hidaka, Saitama 350-1241, Japan

[4]Department of Immunology and Molecular Genetics, Kawasaki Medical School, 577 Matsushima, Kurashiki, Okayama 701-0192, Japan

[5]Department of Medical Technology, Kawasaki University of Medical Welfare, 288 Matsushima, Kurashiki, Okayama 701-0193, Japan

[6]Department of Chromosome Biology, Institute of Molecular Embryplogy and Genetics (IMEG), Kumamoto University, Kumamoto, Japan

[7]Department of Biomedical Science, Graduate School of Medicine, Chiba University, 260-8670, Japan

[8]Department ot Pediatrics, Keio University School of Medicine, Tokyo 160-8582, Japan

[9]Center for Advanced Biomolecular Recognition, Korea Institute of Science and Technology, Seoul, Korea

[10]Department of Molecular Biology, Graduate School of Medical Sciences, Kyushu University, Fukuoka, Japan

[11]Division of Transcriptomics, Medical Institute of Bioregulation, Kyushu University, Fukuoka, Japan

[*]These authors equally contributed to the work

[†]Present address: Faculty of Health and Medical Care, School of Medical Technology, Saitama Medical University, 1397-1 Yamane, Hidaka, Saitama 350-1241, Japan

[§]Present address: Department of Microscopic Anatomy and Developmental Biology, Tokyo Women's Medical University, 8-1, Kawada-cho, Tokyo 112-8681, Japan

[¶]Present address: Department of Design for Medical and Health Care, Faculty of Health and Welfare Services Administration, Kawasaki University of Medical Welfare, 288 Matsushima, Kurashiki, Okayama 701-0193, Japan

[‡]Present address: Department of Clinical Laboratory, Saga University Hospital, 5-1-1 Nabeshima, Saga 849-8501, Japan

Corresponding author: Yuichi Shima, M.D., Ph.D.
Division of Microscopic and Developmetal Anatomy, Department of Anatomy, Kurume University, School of Medicine, 67 Asahi-machi, Kurume-shi, Fukuoka 830-0011, Japan
Tel: +81 942 35 3311 (ext. 3150)
e-mail: yshima@kurume-u.ac.jp

Grants: This work was supported by JSPS (Japan Society for the Promotion of Science) KAKENHI Grant numbers 19K07378 (Y.S.), 23K19458, and 24K09992 (K.M.); Ryobi Teien Memory Foundation (Y.S.); Wesco Scientific Promotion Foundation (Y.S.); Research Project Grant from Kawasaki Medical School (R01B to K.O. and Y.S.); Startup Award for Researchers with Life Events at Kurume University (K.M.); and Grant from Kurume University for the Promotion of female researcher (K.M.).

Abstract

NR5A1 is a nuclear receptor and master regulator of steroidogenic tissue development and steroid hormone biosynthesis in the adrenal glands and gonads. Although NR5A1 is expressed in splenic vascular endothelial cells, its function in the adult spleen remains unclear. Using single-cell transcriptomics in mice, we show that NR5A1-positive endothelial cells are heterogeneous and exhibit distinct phenotypes according to their localization in the splenic sinus or marginal sinus. To assess NR5A1 function, we generated a spleen-specific *Nr5a1* enhancer deletion model. Enhancer loss resulted in reduced spleen size and ablation of the marginal zone and marginal sinus. In addition, 21α-hydroxylase activity in splenic sinusoidal endothelial cells was reduced, particularly in females, leading to decreased levels of adrenocortical steroids in the spleen. Enhancer deletion also induced ectopic lymphatic-like and high endothelial venule-like vasculature similar to those observed in *Nkx2.3*-deficient mice. Consistently, mutation of the NKX2.3-binding motif within the enhancer abolished NR5A1 expression. Together, these findings identify an *Nkx2.3→Nr5a1* regulatory axis essential for spleen-specific endothelial cell differentiation and splenic architecture required for blood filtration and marginal zone formation.

Key words:

NR5A1, enhancer, spleen, red pulp, white pulp, splenic sinus, marginal sinus, marginal zone, lymphocytes, erythrocytes, macrophage

Introduction

The spleen is a central secondary lymphoid organ that performs two key physiological functions. It maintains erythrocyte homeostasis by clearing senescent red blood cells and recycling iron, and it serves as a critical site for immune surveillance and immune responses against blood-borne antigens. The spleen comprises two functionally distinct compartments: red and white pulp. Blood from the splenic artery enters the central artery, which is sheathed by lymphocytes to form the white pulp. A portion of the arterial blood flows into the marginal sinus, located at the interface between the white and red pulp, while the remainder enters the red pulp. In the red pulp, erythrocytes released into open circulation are reclaimed into the large sinusoidal lumen through slits between rod-shaped endothelial cells [1]. Thus, the red pulp serves as a blood filter, where aged or inflexible erythrocytes are trapped and phagocytosed by macrophages[2]. In the white pulp, T cells form periarterial lymphoid sheaths, whereas B cells establish lymphoid follicles that support clonal expansion and immunoglobulin production. The venous sinus surrounding the white pulp, termed the marginal sinus, serves as an entry site for immune cells to migrate into the white pulp[3]. Various subsets of immune cells, including SIGNR1 (CD209b)-positive macrophages, MARCO-positive marginal zone macrophages[4,5], CD169 (SIGLEC-1/sialoadhesin)-positive marginal zone metallophilic macrophages[6,7], and marginal zone B cells[8], reside in the marginal zone and maintain the functional and structural integrity of this unique histological region. Marginal-zone macrophages recognize and phagocytose blood-borne antigens. Marginal-zone B cells rapidly respond to blood-borne antigens by producing IgM and playing distinct roles in follicular B cells, which initiate adaptive responses by undergoing class-switch recombination and producing high-affinity antibodies[9-11]. Recent studies have shown that CD169-positive macrophages migrate to myocardial infarction lesions and contribute to cardiac recovery by suppressing inflammation and regulating fibrosis, highlighting the novel physiological role of marginal-zone macrophages[12].

NR5A1 (also known as Ad4BP or steroidogenic factor-1) is a nuclear receptor critical for the development of steroidogenic tissues, such as the adrenal glands and gonads[13]. NR5A1 is expressed in splenic sinusoidal endothelial cells, and mice with *Nr5a1* gene disruption display a marked reduction in spleen size during fetal stages[14], suggesting impaired splenic blood filtering function. However, because these mice die shortly after birth due to adrenal insufficiency[15], the role of NR5A1 in the adult spleen remains unclear. Recent single-cell transcriptomic analyses of vascular endothelial cells across various mouse tissues have

revealed that genes involved in steroid hormone biosynthesis are expressed in splenic endothelial cells[16]. Although NR5A1 is known to regulate the expression of steroidogenic enzymes in the adrenal cortex[17], the relationship between NR5A1 and steroid hormone production in splenic endothelial cells remains unclear. Furthermore, the physiological significance of steroid hormone production in the spleen remains to be elucidated.

NKX2.3 is a homeobox transcription factor that plays a crucial role in splenic venous sinus formation. *Nkx2.3* (*Nkx2-3*) knockout mice exhibit perinatal lethality and display defects in the spleen and gut-associated lymphoid tissues[18]. In particular, the marginal zone is severely disrupted in *Nkx2.3*-deficient spleens[19,20], and lymphoid cysts filled with lymphocytes and high endothelial venules (HEVs)—structures normally restricted to lymph nodes—develop in knockout spleens[21,22]. These findings establish *Nkx2.3* as essential for spleen-specific vascular architecture.

In this study, we used single-cell transcriptomic analyses to demonstrate that NR5A1-positive endothelial cells in the spleen exhibit distinct gene expression profiles in the splenic and marginal sinuses. We further identify a spleen-specific enhancer that governs *Nr5a1* expression in endothelial cells of both the splenic and marginal sinuses. Through genetic perturbation, we demonstrate that endothelial NR5A1 function is indispensable for establishing spleen-specific vascular identity and marginal zone formation. Furthermore, we identify NKX2.3 as a direct upstream regulator of this enhancer, defining a conserved transcriptional axis that links vascular specialization to immune organ architecture.

Materials and Methods

Mouse strains

Ad4BP-BAC-EGFP mice[23] were used to visualize the cytoplasm of the NR5A1-expressing sinus endothelium and to collect NR5A1-positive endothelial cells from the spleen by cell sorting. StAR/eGFP mice have been described previously[24]. *Nr5a1*$^{\Delta SpE}$ mice were generated using genome editing[25-27]. Guide RNAs targeting the upstream and downstream regions of the SpE were designed using CRISPR Direct (http://crispr.dbcls.jp/), and crRNA, tracrRNA, and Cas9 protein (Integrated DNA Technologies) were mixed and introduced into the fertilized eggs by electroporation (Genome Editor, BEX). For the generation of *Nr5a1*$^{SpE\text{-}R2m}$ mice, guide RNA targeting the R2 sequence in the SpE and donor DNA containing a mutated R2 sequence (R2m) were used. The eggs were then transferred into the oviducts of recipient mothers, and the genotypes of the pups were analyzed by PCR. Integration of the R2m sequence was confirmed by *Bam*HI digestion of the PCR-amplified DNA fragments. Sequences of the guide RNAs and genotyping primers are listed in Supplementary Table 1. All animal protocols were approved by the Animal Care and Use Committee of Kawasaki Medical School and Kurume University School of Medicine.

Single-cell transcriptome analyses of NR5A1^{+} endothelial cells

Ad4BP-BAC-EGFP mice were sacrificed at approximately P70, and their spleens were collected (n = 3, 2 males and 1 female). Spleens were mechanically minced and enzymatically digested with collagenase (Nacalai Tesque). The isolated cells were subjected to fluorescence-activated cell sorting (FACS) using BD FACSAria III (BD) or CytoFLEX SRT (Agilent Biotechnologies). EGFP-positive cells corresponding to NR5A1-expressing vascular endothelial cells were subjected to single-cell RNA sequencing (scRNA-seq) library preparation using the 10x Genomics Chromium Single Cell 3′ Library & Gel Bead Kit v3.1, following the manufacturer's protocol. Libraries from three independent batches were sequenced on an Illumina NovaSeq 6000 platform, and the resulting FASTQ files were processed using Cell Ranger (v9.0.0) with default settings. Reads were aligned to a custom reference genome constructed by appending the enhanced green fluorescent protein (EGFP) gene sequence to the mouse genome assembly (mm10). Initial data quality control and generation of feature-barcode matrices were performed using Cell Ranger's "count" pipeline. Subsequent analyses were performed in R using the Seurat package (v5.1.0)[28]. Cells with fewer than 500 detected genes, more than 6,000 unique molecular identifiers (UMIs), or more than 10% of reads mapping to

166 mitochondrial genes were excluded to eliminate low-quality cells and potential doublets.
167 Potential doublets were further removed using DoubletFinder (v2.0.6)[29], with the doublet
168 formation rate estimated at 7.5% and the optimal pK value determined using the "find.pK"
169 function. After quality filtering was applied, including the EGFP expression criterion, 31,199
170 high-quality cells were retained across the three batches. Gene expression data were normalized
171 using the "NormalizeData" function, and batch effects across samples were simultaneously
172 corrected and integrated using the Harmony algorithm[30]. Dimensionality reduction was
173 performed using principal component analysis (PCA), and the top 30 principal components
174 were used for clustering via the Louvain algorithm at a resolution of 0.1 using the
175 "FindClusters" function. Clusters were visualized using uniform manifold approximation and
176 projection (UMAP) dimensionality reduction implemented via the "RunUMAP" function. From
177 the above analyses, six cell clusters were identified. Differentially expressed genes (DEGs)
178 between clusters were identified using the "FindAllMarkers" function employing the Wilcoxon
179 rank-sum test with the Bonferroni correction for multiple comparisons. Marker genes were
180 defined as those with an average log2 fold change ≥ 1 and an adjusted p-value < 0.01. To
181 functionally annotate the marker genes in each cluster, Gene Ontology (GO) enrichment
182 analysis was performed using the R package clusterProfiler (v 4.17.0)[31]. For each cluster, the
183 top 150 DEGs were selected based on descending log2 fold-change values. These genes were
184 then analyzed using the "compareCluster" and "enrichGO" functions with a q-value cutoff set to
185 0.01. The analysis was conducted across three GO categories: biological processes (BP),
186 molecular functions (MF), and cellular components (CC).
187
188 ***Western blot analyses***
189 Nuclear extracts were prepared from adrenal glands and spleens (Nuclear Extraction Kit,
190 ab113474, Abcam) and quantified using a Qubit Protein Assay (Thermo Fisher Scientific).
191 Forty micrograms of protein was subjected to SDS-polyacrylamide gel electrophoresis and
192 western blot analyses. Primary and secondary antibodies used in the analyses are listed in
193 Supplemental Table 2.
194
195 ***Tissue preparation, histological studies, and immunostaining***
196 Mice were anesthetized with 0.3 mg/kg medetomidine hydrochloride (Nippon Zenyaku Kogyo),
197 4 mg/kg midazolam (Astellas Pharma), and 5 mg/kg butorphanol tartrate (Meiji Seika Pharma).
198 Fresh samples were isolated, and bright-field or fluorescence images of the specimens were

acquired using a stereomicroscope (Evident SZx10 or SZX16). For histological analyses, cardiac perfusion fixation was performed using PBS, followed by 4% paraformaldehyde in PBS. The isolated tissues were fixed by immersion in 4% paraformaldehyde in PBS and subjected to subsequent analyses.

The tissues were embedded in paraffin wax, sectioned at 5-μm thickness, and subjected to hematoxylin and eosin (H&E) and elastica van Gieson (EVG) staining. Images were obtained using BZ-X700 (Keyence), and H&E images were used to measure the area of white pulp and the total area of the spleen using the MZ-X Analyzer 1.3.0.3 (Keyence). For immunostaining, samples were cut into 50-μm-thick sections using a CM3050 S cryotome (Leica). The sections were stained by the free-floating staining method[27]. Primary and secondary antibodies used in this study are listed in Supplementary Table 2. 4′6′-Diamidino-2-phenylindole (DAPI) (Sigma) was used for nuclear staining. Tissue sections were encapsulated in VECTASHIELD Mounting Medium (Vector Laboratories) and photographed using a BZ-X700 (Keyence) or LSM 700 laser-scanning microscope (Zeiss).

Analyses of the circulating hemocytes

Blood smear samples were stained with Giemsa, and the number of erythrocytes containing Howell–Jolly bodies was determined. The erythrocytes were counted using an Olympus Motorized Microscope System BX61 equipped with a DP74 digital camera (Olympus). At least 1,000 erythrocytes were counted in each specimen (n = 4 for each experimental group).

Scanning electron microscopic (SEM) studies

Spleens were fixed by perfusion fixation, followed by interstitial perfusion[32] and immersion fixation using 2.5% glutaraldehyde (TAAB) and 4% paraformaldehyde (Merck) in 0.1 M phosphate buffer (pH 7.4). Tissue blocks (4 × 4 × 2 mm) were trimmed from the fixed organs. After post-fixation with 1% OsO_4, the buffer was replaced with 50% DMSO. Specimens immersed in 50% DMSO were quench-frozen in liquid nitrogen and fractured by mechanical impact. Fixation with 1% OsO_4 was repeated. Then, the specimens were immersed in 2% tannic acid for 16 h and in 2% OsO_4 for 6 h according to the previously reported "tannin-osmium method"[33]. Next, the specimens were dehydrated in increasing concentrations of ethanol and transferred to *t*-butylalcohol, and the soaked samples were sublimed in vacuum and dried while frozen. The specimens were attached, with the fractured surface facing upwards, on a metal stub with a conductive paste. All the specimens were lightly coated with osmium (Neoc-Pro Osmium

232 Coater, Meiwafosis) and platinum (JEC-3000FC Auto Fine Coater, JEOL) by vacuum
233 evaporation. The specimens were observed using an S-3400N scanning electron microscope
234 (Hitachi) at an accelerating voltage of 15 kV.
235
236 ***Bulk mRNA-sequencing, data processing, and differential gene expression analyses***
237 mRNA sequences were analyzed as previously described[26,27]. Briefly, total RNA was prepared
238 from spleens or sorted endothelial cells and subjected to library construction using the Illumina
239 TruSeq Library Construction Kit (Illumina) or NEBNext Ultra RNA Library Prep Kit (New
240 England Biolabs). Libraries were sequenced using a NovaSeq 6000 sequencer (Illumina) with
241 150-bp paired-end reads. After adapter sequences and low-quality sequences were removed
242 using Cutadapt with default parameters, FASTQ files were aligned to the mouse genome
243 (mm10) using STAR (v2.7.3a) with default parameters. FeatureCounts (v2.0.1) and edgeR
244 (v3.28.1) were used to assemble the transcripts and calculate the counts per million (CPM) of
245 each gene using default parameters. DEGs were identified using the criteria of $|\text{Log2FC}| \geq 2$, p
246 < 0.01, and FDR < 0.01, and were subjected to GO analyses using Metascape[34]
247 (https://metascape.org/gp/index.html#/main/step1).
248
249 ***Flow cytometry analyses***
250 Flow cytometry analysis of immune cells in the spleen was performed as previously described[35].
251 The antibodies used for the flow cytometry analyses are listed in Supplemental Table 2.
252
253 ***Measurement of steroid hormones in the spleen***
254 Spleens were collected from the control and ΔSpE mice approximately 10 weeks after birth (n =
255 3 per experimental group). Steroid levels were determined by liquid chromatography-mass
256 spectrometry (LC-MS) following established methods[36,37] and are expressed as nanograms per
257 gram of tissue. The metabolic ratio for each enzymatic reaction was calculated by dividing the
258 metabolite concentration by the precursor concentration.
259
260 ***Sequence data deposition in a public database***
261 All sequencing data were deposited in the Gene Expression Omnibus (GEO) as follows: bulk
262 RNA-seq data of the spleen: GSE303957, bulk RNA-seq data for NR5A1-positive cells isolated
263 by sorting: GSE303956, and scRNA-seq data for NR5A1-positive cells isolated by sorting:
264 GSE303958.

265

266 ***Statistical analyses***

267 At least three animals were used for each experimental group, unless otherwise specified. Data
268 are presented as the mean ± SEM. Statistical comparisons between two groups were performed
269 using the two-tailed Student's *t*-test, and comparisons among multiple groups were conducted
270 using one-way ANOVA followed by the Tukey–Kramer post hoc test; $p < 0.05$ was considered
271 statistically significant.

272

Results

Spatial heterogeneity of NR5A1-expressing endothelial cells in the spleen

NR5A1 has been shown to be expressed in the vascular endothelial cells of the spleen[14]. However, its expression in the spleens of adult mice has not been thoroughly investigated. To address this, we analyzed EGFP expression in the spleens of Ad4BP-BAC-EGFP transgenic mice[23], which faithfully recapitulate endogenous NR5A1 expression. EGFP expression was macroscopically heterogeneous within the spleen and was particularly prominent in the red pulp (Fig. 1A, 1A'). Immunostaining confirmed that EGFP almost completely overlapped with endogenous NR5A1 in the spleen (Fig. S1). Immunostaining of EGFP with the T and B cell markers CD3ε and CD45R, respectively, indicated that EGFP was predominantly expressed in the endothelial cells of the splenic sinusoids within the red pulp (Fig. 1B, 1C). To investigate the location of EGFP-positive cells in more detail, EGFP was compared with several marker proteins for macrophage subtypes (F4/80, macrophage receptor with a collagenous structure [MARCO], and CD169) and a marker for marginal sinus-lining cells (mucosal vascular addressin cell adhesion molecule-1 [MAdCAM-1]). EGFP-positive cells were distributed in the red pulp, where F4/80-positive macrophages are present (arrows in Fig. 1D, D', D''). EGFP-positive cells were also found in the marginal zone, where MARCO-positive macrophages reside (arrowheads in Fig. 1E, E', E''). CD169-positive macrophages (also known as metallophilic macrophages) were located on both the white pulp and red pulp sides of the marginal sinus[7], suggesting that EGFP was expressed in the endothelial cells of the marginal sinus (arrowheads in Fig. 1F, F', F''). MAdCAM-1 has been reported to mark the "lining cells" of the marginal sinus[38], and our analyses also found that MAdCAM-1 is expressed in thin cells, which are closely associated with EGFP-positive cells (arrowheads in Fig. 1G, G', G'') (Fig. S2). Collectively, these data confirm that EGFP is expressed in the endothelial cells of the marginal sinus. Figure 1H summarizes the schematic representation of spatial distribution of NR5A1-positive cells and other cell types in the marginal sinus and marginal zone.

Functional differences between endothelial cells of the splenic sinus and marginal sinus

scRNA-seq analysis of EGFP-positive cells sorted from the spleens of Ad4BP-BAC-EGFP mice was performed. The dimensional reduction of gene expression and clustering of cells collected from three distinct mice (two males and a female) showed almost the same pattern (Fig. S3A), comprising six clusters, including two major ones (clusters 1 and 2 in Fig. 2A). EGFP and endogenous NR5A1 expression was detected in all clusters (Fig. 2B and 2C). Moreover, the

306 sinusoidal endothelial marker *Stab2* was detected across all clusters, including two major
307 clusters (Fig. 2D), confirming the validity of our scRNA-seq analysis. To clarify the
308 relationship between the scRNA-seq results and the spatial distribution of NR5A1-expressing
309 cells observed by immunostaining, we focused on *Star*, which was highly expressed in cluster 1
310 (Fig. 2E), and *Cd34*, which was highly expressed in cluster 2 (Fig. 2F). Immunostaining using
311 Ad4BP-BAC-EGFP mice[23] revealed that CD34 was expressed in the endothelial cells of the
312 marginal sinus (arrows in Fig. 2G). Furthermore, using StAR/eGFP reporter mice[24], in which
313 EGFP expression recapitulates endogenous StAR expression, we observed that CD34-positive
314 and StAR-positive cells were largely mutually exclusive, although a subset of cells co-expressed
315 both markers (arrows in Fig. 2H). Notably, StAR-positive endothelial cells were located outside
316 the marginal zone, where MARCO-positive macrophages are found (Fig. 2I), and within the red
317 pulp, where F4/80-positive macrophages are found (Fig. 2J), strongly suggesting that these cells
318 represent the endothelial cells of the splenic sinus. Thus, cluster 1 in scRNA-seq corresponded
319 to the endothelial cells in the splenic sinus, whereas cluster 2 represented the endothelial cells of
320 the marginal sinus.
321 To elucidate the differences in the properties of endothelial cells between the splenic
322 and marginal sinuses, we performed a more detailed analysis of gene expression in each cluster.
323 Markers commonly expressed in endothelial cells—*Pecam1*, *Cdh5*, *Eng*, and *Erg*—were
324 detected in all clusters, albeit at varying expression levels (Fig. S3B). Gene Ontology (GO)
325 analysis was performed using the top 150 highly expressed genes in each cluster (Fig. 3A, Fig.
326 S4; the gene list is shown in Supplemental Table 3). Cluster 1 was characterized by genes
327 associated with negative chemotaxis (*Flrt2*, *Sema3*d, *Itga9*, *Mmp28*, *Robo2*) and extracellular
328 matrix organization (*Adamts5*, *Col23a1*) (Fig. 3B and Fig. S3C). These genes are also
329 associated with the induction of vasculogenesis, tissue remodeling, and angiogenesis guidance.
330 *Flrt2*, *Sema3d*, and *Robo2* are guidance molecules, and *Jag1* encodes a Notch ligand involved
331 in endothelial fate determination. *Gli3* encodes a transcription factor in the Hedgehog signaling
332 pathway. *Ccbe1*, *Itga9*, *Mmp28*, in addition to *Adamts5* and *Col23a1*, are involved in
333 extracellular matrix degradation and remodeling[39]. In contrast, genes highly expressed in cluster
334 2 were associated with GO terms, such as endothelial cell migration (*Ptp4a3*, *Dll4*, *Col18a1*,
335 *Kdr*, *Id1*, *Adamts9*, *Amotl2*) and angiogenesis (*Esm1*, *Dll4*, *Mcam*, *Emcn*) (Fig. 3A, 3C, Fig.
336 S3D). These terms suggest active angiogenesis. Notably, *Esm1*, *Dll4*, *Kdr*, and *Id1* are known
337 markers of tip cells[40-43]. Moreover, *Esam*, *Col18a1*, *Adamts9*, and *Mcam* have been implicated
338 in cell–cell or cell–matrix adhesion, further pointing to their relevance to angiogenesis[44].

339 Collectively, these results revealed that cells in cluster 1 (splenic sinus) highly express genes
340 involved in vascular patterning and guidance, whereas cells in cluster 2 (marginal sinus) exhibit
341 high expression of genes related to active angiogenesis. Cluster 3 exhibited a high abundance of
342 ribosomal genes (Fig. 3A, Fig. S4A, S4B), suggesting that it represents a population of dead or
343 low-quality cells. Although the developmental relationship between clusters 1 and 2 remains
344 unclear, cluster 4 exhibited an intermediate gene expression profile, suggesting a transitional
345 state between the two major clusters (Fig. 3A, Fig. S4A, S4B). Cluster 5 was characterized by
346 genes related to chromosomal segregation, nuclear division, and sister chromatid segregation,
347 suggesting that these cells were mitotic (Fig. 3A, S4A, S4B). Cluster 6 was enriched in genes
348 related to neutrophil (*Ikzf1*) and lymphocyte differentiation (*Igkc*, *Ly6d*) (Fig. 3A, Fig. S3E, Fig.
349 S4A, S4B), suggesting that this cluster consisted of doublets or contaminating cells, including
350 neutrophils and lymphocytes.
351
352 ***Identification of the SpE in the Nr5a1 gene***
353 We previously identified several tissue-specific enhancers in the *Nr5a1* locus, including the
354 ventromedial hypothalamic nucleus enhancer (VE)[45], fetal adrenal gland enhancer (FAdE)[46],
355 pituitary gonadotrope enhancer (PE)[47], and fetal Leydig cell enhancer (FLE)[48] (Fig. 4A).
356 Furthermore, we demonstrated the functional importance of each enhancer by deleting it from
357 the mouse genome[26,27]. We observed that the sequences of all these enhancers were highly
358 conserved among animal species. Therefore, in this study, we focused on a small region within
359 the fourth intron, whose sequence is conserved among mammalian species, and attempted to
360 elucidate the *in vivo* function by deleting it using CRISPR/Cas9 genome editing (Fig. 4A). We
361 succeeded in deleting a 441-bp region, including the conserved sequence from the mouse
362 genome (Fig. 4B, Fig. S5). This deletion led to the complete disappearance of NR5A1 in the
363 spleen (Fig. 4C). These results indicate that a small region in the fourth intron is indispensable
364 for NR5A1 expression in the spleen. Therefore, we designated this region as the SpE (spleen
365 enhancer) of the *Nr5a1* gene, and homozygous SpE-deletion mice were referred to as ΔSpE
366 mice.
367 Macroscopically, heterozygous deletion of SpE did not markedly affect splenic size.
368 However, the spleens of ΔSpE mice were remarkably smaller than those of the controls (Fig.
369 4D). The spleen, similar to the adrenal gland, exhibits sex differences in size and weight; female
370 spleens are larger and heavier than male spleens[49]. SpE deletion affected the spleen in both
371 males and females, resulting in a significantly lower spleen weight compared to the wild type

372 (Fig. 4E). NR5A1 is essential for the development of the gonads and adrenal glands[15]. However,
373 the adrenal glands, testes, and ovaries were not affected in ΔSpE mice (Fig. S6), indicating that
374 SpE functioned only in the spleen.
375
376 ***Structural and functional abnormality in ΔSpE spleens***
377 HE staining revealed that in wild-type spleens, the white pulp was present as island-like
378 structures within the red pulp. In contrast, in the spleens of ΔSpE mice, the white pulp in both
379 male and female mice was fused and located centrally within the spleen, surrounded by a thin
380 layer of red pulp (Fig. 5A). Interestingly, the measurement of the white pulp-to-red pulp ratio
381 showed that male ΔSpE mice did not differ from wild-type mice, whereas female ΔSpE mice
382 exhibited a significant increase compared to wild-type mice (Fig. 5B). Higher magnification of
383 the HE-stained images of wild-type spleens showed a well-defined marginal zone between the
384 white pulp and red pulp (Fig. 5C) and a marginal sinus at the boundary between the white pulp
385 and the marginal zone (arrows in Fig. 5C). In contrast, in ΔSpE mice, the boundary between the
386 white and red pulp was indistinct, and the structures of the marginal zone and marginal sinus
387 were lost (Fig. 5D). Immunostaining analysis of wild-type spleens demonstrated the spatial
388 arrangement patterns of B and T cells within the white pulp; CD3ε-positive T cells were
389 localized in the central part of the white pulp, and CD45R-positive B cells surrounded the T cell
390 area. Additionally, a marginal zone was observed outside the marginal sinus, which was stained
391 with laminin (Fig. 5E). In contrast, the structures of the marginal zone and marginal sinus were
392 not observed in ΔSpE mice, although the spatial distribution of B and T cells was preserved
393 (Fig. 5F). Notably, the localization patterns of MARCO-positive macrophages in the marginal
394 zone and CD169-positive metallophilic macrophages on the border of the white pulp and
395 marginal sinus were disorganized in SpE heterozygous deletion mice compared with wild-type
396 mice and were entirely lost in ΔSpE mice (Fig. 5G–I). Flow cytometry analyses demonstrated a
397 significant decrease in $CD21^{hi}/CD23^{low/-}$ marginal zone B cells[8] and transitional B cells of type 1
398 (T1B) among the B-lineage cells in ΔSpE spleens (Fig. S7); however, there were no
399 abnormalities in the frequencies of other cell lineages in the spleen (data not shown). These
400 results indicated that the marginal sinus and marginal zone were morphologically and
401 functionally destroyed in the ΔSpE mouse spleen.
402
403 ***Decreased steroidogenic activity in ΔSpE spleen***

404 Bulk RNA sequence analyses were performed to comprehensively explore the functional
405 changes in the spleens of ΔSpE mice. We collected spleens from wild-type and ΔSpE mice
406 (three males and three females per genotype) and performed RNA sequencing. In addition,
407 EGFP-positive cells were isolated from the spleens of Ad4BP-BAC-EGFP mice (three males
408 and three females) using FACS to obtain bulk RNA-seq data. First, we extracted genes whose
409 expression was decreased in the spleens of ΔSpE mice compared to wild-type mice. Notably,
410 the number of downregulated genes in females (1,059) was approximately twice that in males
411 (552). Given this pronounced sex difference, subsequent analyses were performed separately for
412 males and females, and only genes consistently detected in both sexes were retained for further
413 examination.

414 Next, we compared the transcriptomes of whole-spleen tissues from wild-type mice
415 with those of FACS-isolated NR5A1-positive cells (splenic endothelial cells; SECs). We found
416 that 3,481 genes in males and 3,765 genes in females were expressed at higher levels in SECs.
417 Among these, genes that were both highly expressed in SECs and downregulated in ΔSpE
418 spleens numbered 159 in males and 132 in females, with 88 genes shared between the sexes
419 (Fig. 6A, 6B; gene list is shown in Supplemental Table 4). GO analysis of these 88 genes
420 revealed enrichment for terms related to the regulation of adrenal cortical hormone production,
421 suggesting a strong link between adrenal tissue and NR5A1 (Fig. S8). Indeed, the list included
422 *Star* and *Cyp21a1*, both of which are essential for adrenal corticosteroid synthesis (Fig. 6C, 6D,
423 6E).

424 We focused on CYP21A1, an enzyme essential for adrenocortical steroid hormone
425 production and confirmed that *Cyp21a1* expression was almost completely lost in both male and
426 female ΔSpE spleens (Fig. 6E). Splenic steroids were quantified using LC-MS, and the
427 concentrations of 11-deoxycorticosterone and its precursor progesterone were determined (Fig.
428 S9A). The metabolic ratio of these hormones was then calculated, which revealed a slight and
429 considerable reduction in CYP21A1 enzymatic activity in males and females, respectively (Fig.
430 6F).

431 Single-cell transcriptomic analysis further demonstrated that *Star* and *Cyp21a1* were
432 expressed in the endothelial cells of the splenic sinuses, whereas other genes required for
433 adrenal corticosteroid biosynthesis (*Cyp11a1*, *Cyp17a1*, *Hsd3b1*, *Cyp11b1*, *Cyp11b2*) were
434 minimally expressed or not expressed in NR5A1-positive cells (Fig. 6G, Fig. S9B).
435 Collectively, these findings indicate that splenic sinus endothelial cells possess StAR and
436 CYP21A1 activities and contribute to *in situ* corticosteroid synthesis within the spleen.

437 Moreover, the expression of steroidogenic genes in the spleen was dependent on NR5A1
438 expression.
439
440 ***Lymph node-like structures and fibrosis in ΔSpE spleens***
441 Compared with wild-type spleens, ΔSpE spleens showed the upregulation of 798 genes in males
442 and 726 genes in females, with 427 overlapping genes between the sexes (Fig. 7A, 7B; the gene
443 list is shown in Supplemental Table 5). GO analysis of these genes revealed multiple terms
444 related to cell migration and lumen formation (Fig. S10). Notably, this gene list included the
445 lymphatic marker *Lyve1*, as well as *Glycam1* and *Emcn*, which are expressed in HEVs (Fig. 7C,
446 7D). Double immunostaining for LYVE-1 and MECA79 revealed virtually no detectable
447 expression of either marker in the wild-type spleens, whereas LYVE-1-positive lymphatic
448 endothelial cells and MECA79-positive HEVs were clearly observed in the mesenteric lymph
449 nodes. In the spleens of SpE heterozygous mice, MECA79 expression was detected mainly in
450 the red pulp, whereas in ΔSpE mice, distinct LYVE-1-positive lymphatic-like structures and
451 MECA79-positive HEV-like structures were evident (Fig. 7E–H). In contrast, double
452 immunostaining for LYVE-1 and MAdCAM-1 showed that in wild-type spleens, MAdCAM-1
453 was expressed in the lining cells of the marginal sinus, whereas LYVE-1 expression was almost
454 absent. However, in wild-type lymph nodes, both LYVE-1 and MAdCAM-1 were clearly
455 expressed. In the spleens of SpE heterozygous mice, MAdCAM-1 expression was observed in
456 the red pulp, and in ΔSpE mice, distinct LYVE-1-positive lymphatic-like and MAdCAM-1-
457 positive HEV-like structures were apparent, showing a pattern similar to that in the mesenteric
458 lymph nodes (Fig. 7I–L).
459 Scanning electron microscopy showed that in wild-type spleens, endothelial cells
460 were elongated and rod-shaped, with characteristic intercellular slits, whereas in ΔSpE spleens,
461 tall endothelial cells densely lined the vessel lumen, forming HEV-like structures without gaps
462 (Fig. 7M, 7N). Additionally, the loss of fenestrated capillaries, a characteristic of the splenic
463 sinuses, was associated with a significant increase in abnormal red blood cells in the peripheral
464 blood, including Howell–Jolly bodies (Fig. S11). Collectively, these results indicate that ΔSpE
465 spleens lose the identity of the spleen-specific vasculature and acquire a lymph node-like
466 architecture.
467 We also found that the upregulated genes in ΔSpE spleens are related to
468 "extracellular matrix (ECM) organization" and "elastic fiber formation" (Fig. S10). Double
469 immunostaining for F4/80 and laminin revealed that in the spleens of SpE heterozygous mice,

470 small vessels surrounded by laminin-positive basement membranes increased, whereas in ΔSpE
471 mice, these small vessels developed at an even higher density, accompanied by a reduction in
472 F4/80-positive macrophages in the red pulp (Fig. S12A–C). In addition, EVG staining suggested
473 an increase in both collagen and elastic fibers in the spleens of ΔSpE mice. Furthermore, the
474 lymphatic-like structures in the spleens of ΔSpE mice were surrounded by a thin collagen layer
475 (Fig. S12D–I).
476
477 ***NKX2.3 regulates Nr5a1 expression via direct binding to the SpE***
478 Within the SpE, we identified several small subregions with sequences conserved across
479 mammalian species (Fig. S5B). One of these, designated R2, contains a binding motif for the
480 homeobox transcription factor NKX2.3. To test its function, we generated mice in which the R2
481 sequence was replaced with a mutated sequence containing a *Bam*HI restriction site using
482 genome editing, which we named SpE-R2m (Fig. 8A, 8B). The spleens of SpE-R2m mice were
483 markedly smaller than those of wild-type controls (Fig. 8C) and showed complete loss of
484 NR5A1 expression (Fig. 8D–E). Moreover, the marginal sinus and marginal zone were absent
485 (Fig. 8F–H), and ectopic lymphatic- and HEV-like structures were observed, which were
486 essentially indistinguishable from those in ΔSpE mice (Fig. 8I–K). Notably, it has been reported
487 that *Nkx2.3* knockout mice also display small spleens, loss of the marginal zone, and emergence
488 of lymph node-like structures, closely resembling the phenotype of SpE-R2m mice[21,22,50]. In
489 addition, our single-cell transcriptome data indicated that Nkx2.3 is expressed in both the
490 splenic and marginal sinus endothelium (Fig. S13A), and its expression was unaffected by
491 NR5A1 deletion in the spleen (Fig. S13B). Together, these findings strongly suggest that in
492 splenic endothelial cells, NKX2.3 directly regulates *Nr5a1* expression through its binding to
493 SpE.
494

Discussion

Heterogeneity of NR5A1$^+$ endothelial cells in the splenic sinus and marginal sinus

The spleen has two major physiological functions closely associated with the vascular system. First, it acts as a filter that captures foreign substances and senescent red blood cells from circulation. This filtering function is mediated by the unique architecture of the splenic sinus, in which elongated rod-shaped endothelial cells are aligned longitudinally to form large intercellular gaps[1]. The second function is immunity, wherein lymphocytes densely clustered in the white pulp play a central role. The marginal sinus is located at the boundary between the white pulp and marginal zone, and it has been proposed that blood-borne foreign antigens and bacteria are captured by antigen-presenting cells residing in the marginal zone, thereby initiating immune responses[3,8,9,11,51,52].

Although NR5A1 expression in splenic endothelial cells has been reported previously[14], this study is the first to demonstrate its expression in both splenic and marginal sinus endothelial cells. Considering the functional division of the splenic and marginal sinuses described above, it is reasonable to assume that their endothelial cell properties are distinct. Single-cell transcriptomic analyses detected these two populations as separate clusters. Simultaneously, our single-cell analyses also provided novel insights into their functional differences: marginal sinus endothelial cells exhibited higher expression of genes associated with vascular patterning and ECM degradation and remodeling, whereas splenic sinus endothelial cells showed elevated expression of genes related to angiogenesis and cell–substrate adhesion. Moreover, the observation that *Cd34*, a marker highly expressed in immature endothelial cells or endothelial progenitors[53], is more strongly expressed in marginal sinus endothelial cells suggests that they represent a more primitive population, whereas splenic sinus endothelial cells are more differentiated and specialized. The developmental relationship between these two endothelial populations remains an important subject for future investigation.

Downstream genes of Nr5a1 in the spleen

Gene expression analysis of ΔSpE spleens revealed reduced expression of *Star* and *Cyp21a1*, key enzymes in adrenal steroid hormone synthesis. Given that NR5A1 directly regulates steroidogenic enzymes in adrenocortical cells, it is plausible that NR5A1 also directly controls *Star* and *Cyp21a1* expression in the splenic sinus endothelial cells.

Although StAR and CYP21A1 are expressed in NR5A1$^+$ splenic cells, no other enzymes required for complete adrenal steroidogenesis were detected. Nevertheless, adrenal

528 steroids were clearly present in whole-spleen extracts, implying that additional cell types
529 contributed to the remaining enzymatic steps. To our knowledge, this is the first report of
530 adrenal steroid hormone production in the spleen, although its physiological relevance remains
531 to be elucidated.
532 While NR5A1 appears to be indispensable for steroidogenesis in the spleen, the
533 marked disruption of the splenic vascular architecture in ΔSpE mice suggests that NR5A1
534 orchestrates the morphological and functional differentiation of splenic endothelial cells. Thus,
535 NR5A1 may regulate distinct gene networks in the splenic and marginal sinuses. Our single-cell
536 analyses indicated that *Star* and *Cyp21a1* are NR5A1 targets in the splenic sinus, whereas the
537 downstream effectors of NR5A1 in the marginal sinus remain unclear.
538 Immune cells localized in the marginal zone are responsible for mounting immune
539 responses against blood-borne antigens and play a crucial role in the immunological function of
540 the spleen. Our findings suggest that defective formation of the marginal sinus disrupts the
541 microenvironment essential for the development of marginal zone macrophages and marginal
542 zone B cells. Recent studies have shown that macrophages in the marginal zone can migrate and
543 promote cardiac recovery after myocardial infarction by suppressing inflammation and
544 fibrosis[12]. Therefore, NR5A1 is likely to be essential for establishing the tissue organization of
545 the marginal zone that supports these functions. Elucidating how NR5A1 regulates the
546 development and maintenance of the marginal sinus may provide new insights into the
547 maintenance of immune homeostasis and the pathogenesis of immune-related diseases.
548
549 ***Regulation of Nr5a1 gene expression in spleen***
550 Both the spleen and lymph nodes belong to the category of secondary lymphoid organs, and the
551 gut-associated lymphoid tissue (GALT) exhibits a structure similar to that of the lymph nodes.
552 NKX2.3 is expressed in all these lymphoid organs, and analyses of *Nkx2.3* knockout mice have
553 demonstrated that it plays essential roles in each of them. In contrast, NR5A1 expression was
554 restricted to the spleen and was not detected in the lymph nodes or GALT. In this study, we
555 demonstrated that the binding of NKX2.3 to the SpE of the *Nr5a1* gene is indispensable for the
556 expression of *Nr5a1* in the spleen. However, the precise mechanism underlying the spleen-
557 specific activity of SpE remains unclear. It is possible that sequences within SpE other than the
558 R2 region contribute to the spleen-specific regulation of *Nr5a1*. Conversely, although SpE is
559 required for NR5A1 expression in the spleen, we cannot exclude the possibility that additional
560 regulatory regions outside the SpE within the *Nr5a1* locus, known as shadow enhancers, may

561 also be involved in splenic expression. Previous studies have shown that the Polycomb factor
562 M33 participates in the regulation of NR5A1 expression in both the spleen and adrenal gland[54],
563 raising the possibility of a functional relationship between M33 and SpE, which warrants further
564 investigation.
565
566 ***Gene dosage of Nr5a1 and spleen development***
567 Our results demonstrated that heterozygous deletion or mutation of SpE produces a milder
568 phenotype than homozygous deletion, indicating that NR5A1 expression levels are
569 quantitatively important for spleen development. This observation is consistent with that of a
570 previous report and supports the concept that NR5A1 dosage can exert dose-dependent effects
571 on cell differentiation and tissue morphogenesis[55]. However, the phenotype of SpE
572 heterozygous deletion mice was much milder than that of homozygous deletion mice. Similar
573 observations have been reported for other genes, in which the deletion of only one pair of
574 enhancers resulted in a markedly attenuated phenotype compared to homozygous deletion. This
575 phenomenon is generally understood to reflect redundant functions of enhancers[56].
576 Clinically, NR5A1 haploinsufficiency in humans is associated with a spectrum of adrenal and
577 gonadal phenotypes, including varying degrees of adrenal insufficiency and sex
578 development[57,58]. Our data extend this concept to the spleen, demonstrating that subtle
579 reductions in NR5A1 expression can also influence vascular and structural organization, and
580 reinforcing the broader principle that the gene dosage of key transcription factors is a critical
581 determinant of organ development and phenotypic variability.
582 Collectively, these results provide experimental support for the notion that
583 transcription factor dosage is a general and quantitative mechanism that regulates cell
584 differentiation and tissue morphogenesis, with NR5A1 representing a tissue-specific example of
585 this mechanism in the spleen.
586
587 ***Sex difference of steroidogenesis in the spleen***
588 Even in wild-type mice, females have larger spleens and exhibit sex-specific differences in
589 immune cell composition and circulating cytokine levels[49]. In this study, we further found that
590 the effects of NR5A1 deficiency in the spleen differed between sexes, with a significantly
591 increased white pulp-to-red pulp ratio in females. This is consistent with the marked reduction
592 of CYP21A1 expression (and thus 21α-hydroxylase activity) in the red pulp of females.

593 Sex differences in immune function are well established in both mice and humans[59]. Because
594 circulating adrenal steroid hormone levels also show sexual dimorphism, it is plausible that
595 spleen-derived adrenal-type steroid production contributes to these sex differences in immune
596 function and possibly to immune-related pathologies.
597 In our study, the SpE-deficient phenotype was more pronounced in female mice,
598 suggesting that NR5A1-dependent splenic development is regulated in a sex-specific manner.
599 One explanation may be that baseline NR5A1 expression or its developmental timing differs
600 between sexes, such that the partial reduction in females drops more easily below the threshold
601 required for proper endothelial-like cell differentiation and vascular organization. Alternatively,
602 sex hormones, such as estrogen or androgens, may modulate NR5A1-dependent programs
603 during development.
604 These findings are consistent with the broader concept that transcription factor
605 dosage exerts sex-dependent effects on organogenesis. Similar dose- and sex-dependent
606 phenotypes have been reported for other developmental regulators such as SOX9[60] and
607 GATA4/6[61], where small differences in expression lead to divergent outcomes between the
608 sexes. Thus, our results emphasize that both gene dosage and sex-specific context shape the
609 robustness and variability of organ development.
610 From a translational perspective, these findings might be relevant to human NR5A1
611 haploinsufficiency, in which clinical manifestations, including adrenal and gonadal phenotypes,
612 vary between the sexes. Our data suggest that subtle reductions in NR5A1 expression could
613 similarly affect splenic development in a sex-dependent manner, thereby influencing immune
614 function or disease susceptibility.
615
616 **Conclusions**
617 In this study, we demonstrated that NR5A1 expression in splenic endothelial cells is governed
618 by the SpE, which contains a functional NKX2.3-binding motif. Our findings reveal
619 fundamental mechanisms underlying the establishment of organ-specific vascular identity and
620 provide new insights into how transcription factor dosage and sex-specific regulatory programs
621 shape tissue architecture. However, our study has some limitations. The developmental
622 relationship between splenic and marginal sinus endothelial cell populations remains unclear,
623 and the physiological significance of local steroid hormone production in the spleen requires
624 further investigation.
625

The implications of our findings extend beyond basic developmental biology to potential clinical relevance. The disruption of marginal zone architecture in SpE-deficient mice impairs the microenvironment necessary for immune cell localization and function, suggesting that NR5A1 deficiency may influence immune homeostasis and susceptibility to immune-related diseases. The pronounced sex differences observed in SpE-deficient phenotypes, particularly in steroidogenic activity and red and white pulp organization, raise important questions about whether human NR5A1 haploinsufficiency similarly affects splenic development and immune function in a sex-dependent manner. Future studies should focus on identifying the complete spectrum of NR5A1 target genes in both splenic and marginal sinus endothelial cells, elucidating the functional consequences of spleen-derived steroid hormones on local and systemic immunity, and investigating whether NR5A1-dependent splenic development contributes to sex-specific differences in immune responses and disease susceptibility. Understanding these mechanisms may inform therapeutic strategies for immune disorders associated with splenic dysfunction.

640 ***Acknowledgements***
641 We appreciate the technical support provided by the Central Research Center, Kawasaki
642 Medical School, and the Institute for Disease Modeling, Kurume University School of
643 Medicine. We also thank the organizers of the Medical Research Center at Saitama Medical
644 University for providing continuous support throughout this study. This study was supported by
645 the Research Program for the Inter-University Research Network for High-Depth Omics,
646 IMEG, Kumamoto University, Japan. This work was supported in part by the MEXT Promotion
647 of Development of a Joint Usage/Research System Project: Pan-Omics DDRIC, MRCI for
648 High-Depth Omics, CURE: JPMXP1323015486 for MIB, RIIT, and the Autonomous Medical
649 Research Center at Kyushu University. We would like to thank Editage (www.editage.jp) for
650 English language editing.
651
652 ***Author contributions***
653 Conceptualization, Y. S.; Investigation, K. M., K. O., Miki Inoue, T. S., A. Y., Masanori Iseki,
654 Katsuhiko Ishihara, T. M., R. S., Kei-ichirou Ishiguro, J. N., M. H. C., T. B., Y. O., E. K., K. T.,
655 and Y. S.; Resources, T. I.; Format analysis and Writing – Original Draft Preparation, K. M.,
656 K.O., and Y. S.; Writing – Review & Editing, T. S., A. Y., Masanori Iseki, Katsuhiko Ishihara,
657 T. M., Miki Inoue, R. S., Kei-ichirou Ishiguro, M. H. C., T. B., Y. O., E. K., K. T., and Y. S.;
658 Funding Acquisition, K. M., K. O., Y. S., and Supervision, Y. S.
659
660 ***Competing interests***
661 The authors have no conflicts of interest to disclose.
662

663 ***Figure Legends***

664 Figure 1. **EGFP expression in the spleen of Ad4BP-BAC-EGFP mice.**

665 (A, A') Macroscopic view of wild-type and Ad4BP-BAC-EGFP mouse spleens under bright-
666 field (A) and EGFP fluorescence (A') microscopy. The wild-type spleen is outlined with a white
667 dotted line in A'. Bar = 500 μm.

668 (B, C) Immunostaining for EGFP together with CD3ε and CD45R in Ad4BP-BAC-EGFP
669 mouse spleens, shown with (B) or without (C) DAPI nuclear counterstaining. Bar = 100 μm.

670 (D-D'', E-E'', F-F'', G-G'') Immunostaining of EGFP with cell type-specific markers: F4/80
671 (D-D''), MARCO (E-E''), CD169 (F-F''), and MAdCAM-1 (G-G''). Arrows indicate EGFP
672 expression in the endothelial cells of the venous sinuses in the red pulp (splenic sinuses), and
673 arrowheads indicate EGFP expression in the endothelial cells of the venous sinuses at the border
674 between the white pulp and the marginal zone (marginal sinuses). Bar = 50 μm.

675 (H) Schematic illustration of the histological structure of the marginal zone and sinus, showing
676 the cell types observed in this region. RP, red pulp; WP, white pulp.

677

678 Figure 2. **Functional and spatial heterogeneity of EGFP-positive endothelial cells in the**
679 **spleens of Ad4BP-BAC-EGFP mice.**

680 (A) UMAP plot of clusters consisting of EGFP-positive endothelial cells isolated from Ad4BP-
681 BAC-EGFP spleens.

682 (B–F) Feature plots of representative genes expressed in EGFP-positive endothelial cells: *Egfp*
683 (B), *Nr5a1* (C), *Stab2* (D), *Cd34* (E), and *Star* (F).

684 (G) Immunostaining of EGFP and CD34 in Ad4BP-BAC-EGFP spleens.

685 (H–J) Immunostaining of EGFP with CD34 (H), MARCO (I), or F4/80 (J) in StAR/eGFP
686 spleens. Arrows in (G) indicate CD34/EGFP double-positive cells in Ad4BP-BAC-EGFP
687 spleens, whereas arrows in (H) indicate CD34/EGFP double-positive cells in StAR/eGFP
688 spleens. Bar = 100 μm. RP, red pulp; WP, white pulp.

689

690 Figure 3. **Functional characterization of clusters constituting of EGFP-positive endothelial**
691 **cells.**

692 (A) Bubble plot showing the biological processes characterizing each cluster. The top 150
693 highly expressed genes in each cluster were used for GO analysis.

694 (B) Feature plots of representative genes highly expressed in cluster 1: *Flrt2*, *Sema3d*, *Adamts5*,
695 *Ccbe1*, *Itga9*, and *Jag1*.

696 (C) Feature plots of representative genes highly expressed in cluster 2: *Ptp4a3*, *Dll4*, *Kdr*,
697 *Adamts9*, *Esm1*, and *Esam*.
698
699 Figure 4. **Spleen-specific depletion of NR5A1 by deletion of the spleen enhancer (SpE) of**
700 **the *Nr5a1* gene.**
701 (A) Schematic representation of the *Nr5a1* gene structure and sequence conservation among
702 mammals. Gray boxes indicate previously identified enhancers, including fetal Leydig enhancer
703 (FLE), fetal adrenal enhancer (FAdE), ventromedial hypothalamus enhancer (VE), and pituitary
704 enhancer (PE). The yellow box indicates the spleen enhancer (SpE) located in intron 4. Arrows
705 (SpE-Fw and SpE-Re) denote genotyping primers.
706 (B) PCR-based genotyping of SpE-deleted mice. The wild-type allele yields a 655-bp fragment,
707 whereas the SpE-deleted allele yields a 213-bp fragment.
708 (C) Loss of NR5A1 expression in the spleens of ΔSpE mice. Western blot analysis of NR5A1
709 and LaminB1 in nuclear extracts from spleens of wild-type (+/+), heterozygous (+/-), and
710 homozygous (-/-) SpE-deleted mice.
711 (D) Gross morphology of spleens from wild-type (+/+), heterozygous (+/-), and homozygous (-
712 /-) SpE-deleted mice.
713 (E) Spleen weight-to-body weight ratio in each genotype and sex (mean ± SE). Sample size:
714 male wild-type, n = 12; male ΔSpE, n = 6; female wild-type n = 9; female ΔSpE, n = 5. $p < 0.01$
715 (**).
716
717 Figure 5. **Morphological analysis of ΔSpE spleens.**
718 (A) Hematoxylin and eosin (HE) staining of spleens from each genotype and sex. Scale bar = 2
719 mm
720 (B) White pulp-to-red pulp area ratios in each genotype and sex. Sample sizes: male wild-type,
721 n = 6; male ΔSpE, n = 4; female wild-type n = 5; female ΔSpE, n = 3. $p < 0.01$ (**).
722 (C, D) High-magnification HE-stained images of wild-type (WT) and ΔSpE spleens. Arrows
723 indicate marginal sinuses. Scale bar = 100 μm.
724 (E, F) Immunostaining of CD45R, CD3ε, and laminin in wild-type (WT) and ΔSpE spleens. RP,
725 red pulp; WP, white pulp; MZ, marginal zone. Scale bar = 100 μm.
726 (G., H., I) Immunostaining for MARCO and CD169 in wild-type (WT), heterozygous (Het), and
727 homozygous (ΔSpE) spleens. Scale bar = 100 μm.
728

729 Figure 6. **Downregulated genes in ΔSpE spleens.**

730 (A) Schematic representation of the strategy for gene expression analyses. Comparison of gene
731 expression between wild-type (WT) spleens and sorted NR5A1^{+} sinusoidal endothelial cells
732 (SECs) identified genes enriched in SECs (Up in SEC). Comparison between WT and ΔSpE
733 spleens identified genes downregulated in ΔSpE (Down in ΔSpE). Genes included in both
734 categories (Up in SEC and Down in ΔSpE) were extracted for each sex.

735 (B) Venn diagram showing overlapping (Up in SEC and Down in ΔSpE) genes in both sexes.

736 (C) Schematic representation of steroid biosynthetic pathways, including steroidogenic
737 enzymes, precursors, and metabolites. Enzymes indicated in blue are among 88 genes identified
738 in (B). Metabolites indicated in red represent corticosteroid hormones and their precursors.

739 (D) Volcano plot analysis of gene expression in WT and ΔSpE spleens. Genes in red indicate
740 representative genes downregulated in ΔSpE.

741 (E) Expression levels of *Cyp21a1* gene in WT and ΔSpE spleens in each sex, showing as counts
742 per million (CPM). $p < 0.01$ (**).

743 (F) Metabolic activity of 21α-hydroxylase, assessed by precursor and metabolite concentrations
744 in WT and ΔSpE spleens of each sex, determined by gas chromatography-mass spectrometry
745 (GC-MS). $p < 0.05$ (*).

746 (G) Feature plot of *Cyp21a1* expression in a UMAP presentation of NR5A1^{+} endothelial cells in
747 the spleen.

748

749 Figure 7. **Upregulated genes in ΔSpE spleens.**

750 (A) Schematic representation of the strategy for gene expression analyses. Comparison of gene
751 expression between wild-type (WT) and ΔSpE spleens identified genes upregulated in ΔSpE
752 (Up in ΔSpE).

753 (B) Venn diagram showing (Up in ΔSpE) genes in both sexes.

754 (C) Volcano plot analysis of gene expression in WT and ΔSpE spleens. Genes in red indicate
755 representative genes upregulated in ΔSpE.

756 (D) Expression levels of *Lyve1*, *Glycam1*, *and Emcn* genes in WT and ΔSpE spleens in each
757 sex, showing as counts per million (CPM). $p < 0.01$ (**).

758 (E, F, G, H) Immunostaining of LYVE-1 and MECA79 in WT, heterozygous (Het), ΔSpE
759 spleens and wild-type mesenteric lymph node (WT mLN). Scale bar = 100 μm.

760 (I, J, K, L) Immunostaining of LYVE-1 and MAdCAM-1 in WT, heterozygous (Het), ΔSpE
761 spleens and wild-type mesenteric lymph node (WT mLN). Scale bar = 100 μm.

762 (M, N) Scanning electron microscopy (SEM) images of WT and ΔSpE spleens. Scale bar = 50
763 μm.
764
765 Figure 8. **NKX2.3 regulates *Nr5a1* gene expression in the spleen via direct binding to SpE.**
766 (A) Schematic representation of a mutation induced in R2 sequence in SpE. The yellow box
767 indicates SpE, and arrows indicate genotyping primers (SpE-Fw and SpE-Re). The red open
768 rectangle indicates the R2 sequence, and asterisks indicate the NKX2.3-binding motif. Mutated
769 R2 sequence (R2m) contains *Bam*HI restriction element (*Bam*HI-RE). The consensus sequence
770 for human NKX2-3 binding was searched in JASPAR (https://jaspar.genereg.net/) and is shown
771 in PWM format.
772 (B) PCR-based genotyping of SpE-deleted mice. The wild-type allele yielded a 655-bp
773 fragment, whereas the SpE-R2m allele yielded 429-bp and 225-bp fragments.
774 (C) Gross morphology of spleens from wild-type (+/+) and homozygous mutation in SpE (SpE-
775 R2m) mice. Scale bar = 2 mm.
776 (D, E) Immunostaining of NR5A1 in WT and SpE-R2m spleens. Scale bar = 50 μm.
777 (F, G, H) Immunostaining of CD34 and MARCO in WT, heterozygous (Het) and homozygous
778 SpE-R2m spleens. Scale bar = 100 μm.
779 (I, J, K) Immunostaining of CD34 and MARCO in WT, heterozygous (Het), and homozygous
780 SpE-R2m spleens. Scale bar = 100 μm.
781

782 Supplemental Figure 1. **Comparison of endogenous NR5A1 and EGFP expression in the**
783 **spleens of Ad4BP-BAC-EGFP mice.**
784 Double immunostaining for NR5A1 (red) and EGFP (green) and nuclear counterstaining with
785 DAPI (blue) were performed on spleen sections from Ad4BP-BAC-EGFP mice. Images of the
786 same field are as follows: (A) NR5A1 channel; (B) EGFP channel; (C) merged NR5A1 and
787 EGFP; and (D) merged NR5A1, EGFP, and DAPI. Magnified views of the regions including the
788 marginal sinus are presented as A', B', C', and D', with arrows indicating endothelial cells of
789 the marginal sinus. Likewise, enlarged views of regions including the splenic sinus are shown as
790 A'', B'', C'', and D'', with arrowheads indicating the endothelial cells of the splenic sinus.
791 Scale bar = 50 μm.
792
793 Supplemental Figure 2 **Spatial relationship between EGFP-positive cells and MAdCAM-1-**
794 **positive cells in the spleen of Ad4BP-BAC-EGFP mice.**
795 (A) Immunofluorescence image of MAdCAM-1, EGFP, and Laminin, together with DAPI
796 nuclear staining, in the spleens of Ad4BP-BAC-EGFP mice. The region outlined by the yellow
797 box is shown enlarged in panel B. Scale bar = 50 μm The image in panel B is further separated
798 into individual channels: MAdCAM-1 (red) in panel C; laminin (white) in panel D; merged
799 MAdCAM-1 and EGFP in panel E; EGFP (green) in panel F; and DAPI (blue) in panel G.
800 Dotted lines in panels C, D, F, and G indicate MAdCAM-1-positive cells. (H) Line plot
801 generated along the direction indicated by the arrow in Panel B. The plot shows that EGFP-
802 positive cells (green) are adjacent to MAdCAM-1-positive cells (red). Scale bar = 10 μm
803
804 Supplemental Figure 3. **Gene expression profiles in each cluster of NR5A1+ cells in the**
805 **spleens of Ad4BP-BAC-EGFP mice.**
806 (A) UMAP plot of cells from three mice (two males and one female) after merging the datasets,
807 with cells colored according to their individual origin.
808 (B) Feature plots of representative genes commonly expressed in clusters 1 and 2.
809 (C) Feature plots of representative genes that were highly expressed in cluster 1.
810 (D) Feature plots of representative genes highly expressed in cluster 2.
811 (E) Feature plots of representative genes highly expressed in cluster 6 (highlighted with red
812 circles).
813

814 Supplemental Figure 4. **GO analysis of genes enriched in each cluster of NR5A1^{+} sinus**
815 **endothelial cells in the spleens of Ad4BP-BAC-EGFP mice.**
816 (A) Bubble plot showing the molecular functions associated with each cluster identified by
817 scRNA-seq in EGFP^{+} sinus endothelial cells. (B) Bubble plot showing the cellular components
818 associated with each cluster identified by scRNA-seq of EGFP^{+} sinus endothelial cells. Gene
819 Ontology (GO) analysis was performed using the top 150 highly expressed genes in each
820 cluster.
821
822 Supplemental Figure 5. **Schematic illustration of the SpE deletion by CRISPR/Cas9.**
823 (A) Two guide RNAs were designed to target the upstream and downstream regions of the SpE.
824 Arrows (SpE-Fw and SpE-Re) indicate the positions of the genotyping PCR primers. Nucleotide
825 sequences surrounding the guide RNA target sites are shown (WT, wild type; de, SpE deletion).
826 Guide RNA target sequences are shown in red, and PAM sequences are underlined.
827 (B) Alignment of the nucleotide sequences of SpE regions in mice, rats, rabbits, pigs, and dogs
828 using MAFFT (https://mafft.cbrc.jp/alignment/software/). Asterisks indicate nucleotides
829 conserved among all species. Guide RNA target sequences are shown in red, and PAM
830 sequences are underlined. Nucleotides boxed in red indicate the R2 sequence, the mutation of
831 which abolished enhancer activity.
832
833 Supplemental Figure 6. **Morphology of NR5A1-expressing organs other than the spleen in**
834 **ΔSpE mice.**
835 (A) Gross morphology of the adrenal glands in wild-type (WT) and ΔSpE mice.
836 (B) Gross morphology of the ovaries in wild-type (WT) and ΔSpE mice.
837 (C) Gross morphology of the testes in wild-type (WT) and ΔSpE mice.
838 Scale bar = 2 mm.
839
840 Supplemental Figure 7. **Flow cytometric analysis of splenic immune cells in ΔSpE mice.**
841 (A) Representative flow cytometry plot of the spleen. B: B cells (CD19^{+}), MZB: marginal zone
842 B cells (CD19^{+}CD21/35^{high}CD23$^{low/-}$), FoB: follicular B cells (CD19^{+}CD21/35^{high}CD23^{high}),
843 T1B: Transitional B cells of type1 (CD19^{+}CD21/35^{-}CD23^{-}), T2B: transitional B cells of type 2
844 (CD19^{+}CD23^{+}CD21/35^{+}IgM^{+}).
845 (B) Flow cytometry of B-cell subsets isolated from the spleen of a wild-type mouse.
846 CD21/35^{high}CD23$^{low/-}$ (marginal zone B cells) cells constitute 6.91% of CD19^{+} B cells.

847 (C) Flow cytometry of B-cell subsets isolated from the spleen of an SpE heterozygous mouse.
848 CD21/35^{high}CD23$^{low/-}$ cells constitute 7.38% of CD19^{+}B cells.
849 (D) Flow cytometry analysis of B-cell subsets isolated from the spleen of a ΔSpE mouse.
850 CD21/35^{high}CD23$^{low/-}$ cells constituted 0.66% of CD19^{+}B cells.
851 (E) Frequencies of B-cell subsets in the spleen: B: B cells, FoB: follicular B cells, T1B:
852 transitional B cells of type 1, T2B: transitional B cells of type 2, MZB: marginal zone B cells,
853 WT: wild-type: Het, heterozygous deletion of SpE, ΔSpE: deletion of SpE,*: $p < 0.05$, ns: not
854 significant.
855
856 Supplemental Figure 8. **GO analysis of genes downregulated in the spleens of ΔSpE mice.**
857 (A) Biological processes associated with the downregulated genes in ΔSpE spleens.
858 (B) Tissue specificity of genes downregulated in ΔSpE spleens.
859 (C) Transcription factors predicted to regulate the genes downregulated in ΔSpE spleens.
860
861 Supplemental Figure 9. **Steroid levels and expression of steroidogenic genes in the spleen.**
862 (A) The concentrations of progesterone and 11-deoxycorticosterone were measured by LC-MS.
863 M, male; F, female; WT, wild type.
864 (B) Feature plots showing the expression of the genes required for adrenal steroid production.
865 *Star* and *Cyp21a1* were expressed in cluster 1, whereas the expression of the other genes was
866 very low or undetectable (ND).
867
868 Supplemental Figure 10. **Upregulated genes the spleens of ΔSpE mice.**
869 Biological processes identified by GO analysis of genes upregulated in the spleen of ΔSpE
870 mice.
871
872 Supplemental Figure 11. **Abnormal peripheral erythrocytes in ΔSpE mice.**
873 (A) Giemsa-stained peripheral blood samples from control male mouse.
874 (B) Giemsa-stained peripheral blood samples from a male ΔSpE mice. Arrows indicate
875 abnormal erythrocytes containing Howell–Jolly bodies. Scale bar = 20 μm.
876 (C) The proportion of erythrocytes containing Howell–Jolly bodies in control and ΔSpE mice of
877 each sex. At least 1,000 erythrocytes were examined per specimen (n = 4). $p < 0.01$ (**).
878
879 Supplemental Figure 12. **Increased ECM expression in the spleens of ΔSpE mice.**

880 (A–C) Double immunostaining for F4/80 (red) and Laminin (green) with nuclear
881 counterstaining using DAPI (blue) in the spleen sections. WT, wild type; Het, SpE
882 heterozygous. Scale bar = 100 μm.
883 (D–F) Hematoxylin and eosin (HE) staining of spleens from WT and ΔSpE mice. Arrowheads
884 in (E) and (F) indicate ectopic lymphatic-like structures filled with lymphocytes.
885 (G–I) Elastica van Gieson (EVG) staining of spleens from WT and ΔSpE mice. The arrowheads
886 in (H) and (I) indicate ectopic lymphatic-like structures filled with lymphocytes. Scale bar = 50
887 μm.
888
889 Supplemental Figure 13. ***Nkx2-3* expression in the spleens of ΔSpE mice.**
890 (A) Feature plot showing *Nkx2-3* expression in NR5A1^{+} cells isolated from the spleens of
891 Ad4BP-BAC-EGFP mice. *Nkx2-3* is expressed in clusters 1 and 2.
892 (B) *Nkx2-3* expression in the spleens of wild-type (WT) and ΔSpE mice of both sexes, as
893 revealed by mRNA-sequence analysis. Expression levels are expressed as counts per million
894 (CPM).
895

896 ***References***

897 1. MacDonald, I.C., Ragan, D.M., Schmidt, E.E., and Groom, A.C. (1987). Kinetics of red
898 blood cell passage through interendothelial slits into venous sinuses in rat spleen,
899 analyzed by in vivo microscopy. Microvasc Res *33*, 118-134. 10.1016/0026-
900 2862(87)90011-2.

901 2. Bratosin, D., Mazurier, J., Tissier, J.P., Estaquier, J., Huart, J.J., Ameisen, J.C., Aminoff,
902 D., and Montreuil, J. (1998). Cellular and molecular mechanisms of senescent erythrocyte
903 phagocytosis by macrophages. A review. Biochimie *80*, 173-195. 10.1016/s0300-
904 9084(98)80024-2.

905 3. Mebius, R.E., and Kraal, G. (2005). Structure and function of the spleen. Nat Rev
906 Immunol *5*, 606-616. 10.1038/nri1669.

907 4. Geijtenbeek, T.B., Groot, P.C., Nolte, M.A., van Vliet, S.J., Gangaram-Panday, S.T., van
908 Duijnhoven, G.C., Kraal, G., van Oosterhout, A.J., and van Kooyk, Y. (2002). Marginal
909 zone macrophages express a murine homologue of DC-SIGN that captures blood-borne
910 antigens in vivo. Blood *100*, 2908-2916. 10.1182/blood-2002-04-1044.

911 5. Elomaa, O., Kangas, M., Sahlberg, C., Tuukkanen, J., Sormunen, R., Liakka, A., Thesleff,
912 I., Kraal, G., and Tryggvason, K. (1995). Cloning of a novel bacteria-binding receptor
913 structurally related to scavenger receptors and expressed in a subset of macrophages. Cell
914 *80*, 603-609. 10.1016/0092-8674(95)90514-6.

915 6. Kraal, G., and Janse, M. (1986). Marginal metallophilic cells of the mouse spleen
916 identified by a monoclonal antibody. Immunology *58*, 665-669.

917 7. Munday, J., Floyd, H., and Crocker, P.R. (1999). Sialic acid binding receptors (siglecs)
918 expressed by macrophages. J Leukoc Biol *66*, 705-711. 10.1002/jlb.66.5.705.

919 8. Martin, F., and Kearney, J.F. (2002). Marginal-zone B cells. Nat Rev Immunol *2*, 323-
920 335. 10.1038/nri799.

921 9. Borges da Silva, H., Fonseca, R., Pereira, R.M., Cassado Ados, A., Alvarez, J.M., and
922 D'Imperio Lima, M.R. (2015). Splenic macrophage subsets and their function during
923 blood-borne infections. Front Immunol *6*, 480. 10.3389/fimmu.2015.00480.

924 10. Koppel, E.A., Litjens, M., van den Berg, V.C., van Kooyk, Y., and Geijtenbeek, T.B.
925 (2008). Interaction of SIGNR1 expressed by marginal zone macrophages with marginal
926 zone B cells is essential to early IgM responses against Streptococcus pneumoniae. Mol
927 Immunol *45*, 2881-2887. 10.1016/j.molimm.2008.01.032.

928 11. Bronte, V., and Pittet, M.J. (2013). The spleen in local and systemic regulation of

929 immunity. Immunity *39*, 806-818. 10.1016/j.immuni.2013.10.010.
930 12. Ismahil, M.A., Zhou, G., Rajasekar, S., Gao, M., Bansal, S.S., Patel, B., Limdi, N., Xie,
931 M., Antipenko, S., Rokosh, G., et al. (2025). Splenic CD169(+)Tim4(+) marginal
932 metallophilic macrophages are essential for wound healing after myocardial infarction.
933 Circulation. 10.1161/CIRCULATIONAHA.124.071772.
934 13. Parker, K.L., and Schimmer, B.P. (1997). Steroidogenic factor 1: a key determinant of
935 endocrine development and function. Endocr Rev *18*, 361-377. 10.1210/edrv.18.3.0301.
936 14. Morohashi, K., Tsuboi-Asai, H., Matsushita, S., Suda, M., Nakashima, M., Sasano, H.,
937 Hataba, Y., Li, C.L., Fukata, J., Irie, J., et al. (1999). Structural and functional
938 abnormalities in the spleen of an mFtz-F1 gene-disrupted mouse. Blood *93*, 1586-1594.
939 15. Luo, X., Ikeda, Y., and Parker, K.L. (1994). A cell-specific nuclear receptor is essential
940 for adrenal and gonadal development and sexual differentiation. Cell *77*, 481-490.
941 10.1016/0092-8674(94)90211-9.
942 16. Kalucka, J., de Rooij, L., Goveia, J., Rohlenova, K., Dumas, S.J., Meta, E., Conchinha,
943 N.V., Taverna, F., Teuwen, L.A., Veys, K., et al. (2020). Single-cell transcriptome atlas of
944 murine endothelial cells. Cell *180*, 764-779 e720. 10.1016/j.cell.2020.01.015.
945 17. Morohashi, K.I., and Omura, T. (1996). Ad4BP/SF-1, a transcription factor essential for
946 the transcription of steroidogenic cytochrome P450 genes and for the establishment of
947 the reproductive function. FASEB J *10*, 1569-1577. 10.1096/fasebj.10.14.9002548.
948 18. Pabst, O., Zweigerdt, R., and Arnold, H.H. (1999). Targeted disruption of the homeobox
949 transcription factor Nkx2-3 in mice results in postnatal lethality and abnormal
950 development of small intestine and spleen. Development *126*, 2215-2225.
951 10.1242/dev.126.10.2215.
952 19. Wang, C.C., Biben, C., Robb, L., Nassir, F., Barnett, L., Davidson, N.O., Koentgen, F.,
953 Tarlinton, D., and Harvey, R.P. (2000). Homeodomain factor Nkx2-3 controls regional
954 expression of leukocyte homing coreceptor MAdCAM-1 in specialized endothelial cells
955 of the viscera. Dev Biol *224*, 152-167. 10.1006/dbio.2000.9749.
956 20. Tarlinton, D., Light, A., Metcalf, D., Harvey, R.P., and Robb, L. (2003). Architectural
957 defects in the spleens of Nkx2-3-deficient mice are intrinsic and associated with defects
958 in both B cell maturation and T cell-dependent immune responses. J Immunol *170*, 4002-
959 4010. 10.4049/jimmunol.170.8.4002.
960 21. Kellermayer, Z., Labadi, A., Czompoly, T., Arnold, H.H., and Balogh, P. (2011). Absence
961 of Nkx2-3 homeodomain transcription factor induces the formation of LYVE-1-positive

endothelial cysts without lymphatic commitment in the spleen. J Histochem Cytochem *59*, 690-700. 10.1369/0022155411410061.

22. Gabris, F., Kiss, G., Szirmay, B., Szomor, A., Berta, G., Jakus, Z., Kellermayer, Z., and Balogh, P. (2023). Absence of Nkx2-3 induces ectopic lymphatic endothelial differentiation associated with impaired extramedullary stress hematopoiesis in the spleen. Front Cell Dev Biol *11*, 1170389. 10.3389/fcell.2023.1170389.

23. Miyabayashi, K., Tokunaga, K., Otake, H., Baba, T., Shima, Y., and Morohashi, K. (2015). Heterogeneity of ovarian theca and interstitial gland cells in mice. PLoS One *10*, e0128352. 10.1371/journal.pone.0128352.

24. Sasaki, G., Ishii, T., Jeyasuria, P., Jo, Y., Bahat, A., Orly, J., Hasegawa, T., and Parker, K.L. (2008). Complex role of the mitochondrial targeting signal in the function of steroidogenic acute regulatory protein revealed by bacterial artificial chromosome transgenesis in vivo. Mol Endocrinol *22*, 951-964. 10.1210/me.2007-0493.

25. Jinek, M., Chylinski, K., Fonfara, I., Hauer, M., Doudna, J.A., and Charpentier, E. (2012). A programmable dual-RNA-guided DNA endonuclease in adaptive bacterial immunity. Science *337*, 816-821. 10.1126/science.1225829.

26. Shima, Y., Miyabayashi, K., Mori, T., Ono, K., Kajimoto, M., Cho, H.L., Tsuchida, H., Uenoyama, Y., Tsukamura, H., Suzuki, K., et al. (2022). Intronic enhancer is essential for Nr5a1 expression in the pituitary gonadotrope and for postnatal development of male reproductive organs in a mouse model. Int J Mol Sci *24*, 192. 10.3390/ijms24010192.

27. Shima, Y., Miyabayashi, K., Sato, T., Suyama, M., Ohkawa, Y., Doi, M., Okamura, H., and Suzuki, K. (2018). Fetal Leydig cells dedifferentiate and serve as adult Leydig stem cells. Development *145*, dev169136. 10.1242/dev.169136.

28. Hao, Y., Stuart, T., Kowalski, M.H., Choudhary, S., Hoffman, P., Hartman, A., Srivastava, A., Molla, G., Madad, S., Fernandez-Granda, C., and Satija, R. (2024). Dictionary learning for integrative, multimodal and scalable single-cell analysis. Nat Biotechnol *42*, 293-304. 10.1038/s41587-023-01767-y.

29. McGinnis, C.S., Murrow, L.M., and Gartner, Z.J. (2019). DoubletFinder: Doublet detection in single-cell RNA sequencing data using artificial nearest neighbors. Cell Syst *8*, 329-337 e324. 10.1016/j.cels.2019.03.003.

30. Korsunsky, I., Millard, N., Fan, J., Slowikowski, K., Zhang, F., Wei, K., Baglaenko, Y., Brenner, M., Loh, P.R., and Raychaudhuri, S. (2019). Fast, sensitive and accurate integration of single-cell data with Harmony. Nat Methods *16*, 1289-1296.

995 10.1038/s41592-019-0619-0.
996 31. Wu, T., Hu, E., Xu, S., Chen, M., Guo, P., Dai, Z., Feng, T., Zhou, L., Tang, W., Zhan, L.,
997 et al. (2021). clusterProfiler 4.0: A universal enrichment tool for interpreting omics data.
998 Innovation (Camb) *2*, 100141. 10.1016/j.xinn.2021.100141.
999 32. Gamliel, H., Golomb, H.M., Avinoah, E., Gurfel, D., and Polliack, A. (1986). Topical
1000 modes in the preparation of human spleen specimens for routine scanning electron
1001 microscopy studies. Scan Electron Microsc *Pt 3*, 1039-1050.
1002 33. Fujita, T. (1974). A scanning electron microscope study of the human spleen. Arch Histol
1003 Jpn *37*, 187-216. 10.1679/aohc1950.37.187.
1004 34. Zhou, Y., Zhou, B., Pache, L., Chang, M., Khodabakhshi, A.H., Tanaseichuk, O., Benner,
1005 C., and Chanda, S.K. (2019). Metascape provides a biologist-oriented resource for the
1006 analysis of systems-level datasets. Nat Commun *10*, 1523. 10.1038/s41467-019-09234-
1007 6.
1008 35. Yahagi, A., Iseki, M., Yaku, K., Nakagawa, T., Itoh, M., Mukai, T., and Ishihara, K. (2025).
1009 Aberrant humoral immune responses and intestinal homeostasis in Cd38 Bst1 double
1010 knockout mice. Immunohorizons *9*, vlaf029. 10.1093/immhor/vlaf029.
1011 36. Han, S., Baba, T., Yanai, S., Byun, D.J., Morohashi, K.I., Kim, J.H., and Choi, M.H.
1012 (2021). GC-MS-based metabolic signatures reveal comparative steroidogenic pathways
1013 between fetal and adult mouse testes. Andrology *9*, 400-406. 10.1111/andr.12893.
1014 37. Noh, J., Lee, C., Kim, J.H., Myung, S.W., and Choi, M.H. (2023). LC-MS based
1015 simultaneous profiling of adrenal hormones of steroids, catecholamines, and
1016 metanephrines. J Lipid Res *64*, 100453. 10.1016/j.jlr.2023.100453.
1017 38. Kraal, G., Schornagel, K., Streeter, P.R., Holzmann, B., and Butcher, E.C. (1995).
1018 Expression of the mucosal vascular addressin, MAdCAM-1, on sinus-lining cells in the
1019 spleen. Am J Pathol *147*, 763-771.
1020 39. Libby, J.R., Royce, H., Walker, S.R., and Li, L. (2024). The role of extracellular matrix
1021 in angiogenesis: Beyond adhesion and structure. Biomater Biosyst *15*, 100097.
1022 10.1016/j.bbiosy.2024.100097.
1023 40. Goveia, J., Rohlenova, K., Taverna, F., Treps, L., Conradi, L.C., Pircher, A., Geldhof, V.,
1024 de Rooij, L., Kalucka, J., Sokol, L., et al. (2020). An integrated gene expression landscape
1025 profiling approach to identify lung tumor endothelial cell heterogeneity and angiogenic
1026 candidates. Cancer Cell *37*, 21-36 e13. 10.1016/j.ccell.2019.12.001.
1027 41. Geldhof, V., de Rooij, L., Sokol, L., Amersfoort, J., De Schepper, M., Rohlenova, K.,

1028 Hoste, G., Vanderstichele, A., Delsupehe, A.M., Isnaldi, E., et al. (2022). Single cell atlas
1029 identifies lipid-processing and immunomodulatory endothelial cells in healthy and
1030 malignant breast. Nat Commun *13*, 5511. 10.1038/s41467-022-33052-y.
1031 42. Kang, B., Camps, J., Fan, B., Jiang, H., Ibrahim, M.M., Hu, X., Qin, S., Kirchhoff, D.,
1032 Chiang, D.Y., Wang, S., et al. (2022). Parallel single-cell and bulk transcriptome analyses
1033 reveal key features of the gastric tumor microenvironment. Genome Biol *23*, 265.
1034 10.1186/s13059-022-02828-2.
1035 43. Zeng, Q., Mousa, M., Nadukkandy, A.S., Franssens, L., Alnaqbi, H., Alshamsi, F.Y., Safar,
1036 H.A., and Carmeliet, P. (2023). Understanding tumour endothelial cell heterogeneity and
1037 function from single-cell omics. Nat Rev Cancer *23*, 544-564. 10.1038/s41568-023-
1038 00591-5.
1039 44. Francavilla, C., Maddaluno, L., and Cavallaro, U. (2009). The functional role of cell
1040 adhesion molecules in tumor angiogenesis. Semin Cancer Biol *19*, 298-309.
1041 10.1016/j.semcancer.2009.05.004.
1042 45. Shima, Y., Zubair, M., Ishihara, S., Shinohara, Y., Oka, S., Kimura, S., Okamoto, S.,
1043 Minokoshi, Y., Suita, S., and Morohashi, K. (2005). Ventromedial hypothalamic nucleus-
1044 specific enhancer of Ad4BP/SF-1 gene. Mol Endocrinol *19*, 2812-2823.
1045 10.1210/me.2004-0431.
1046 46. Zubair, M., Ishihara, S., Oka, S., Okumura, K., and Morohashi, K. (2006). Two-step
1047 regulation of Ad4BP/SF-1 gene transcription during fetal adrenal development: initiation
1048 by a Hox-Pbx1-Prep1 complex and maintenance via autoregulation by Ad4BP/SF-1. Mol
1049 Cell Biol *26*, 4111-4121. 10.1128/MCB.00222-06.
1050 47. Shima, Y., Zubair, M., Komatsu, T., Oka, S., Yokoyama, C., Tachibana, T., Hjalt, T.A.,
1051 Drouin, J., and Morohashi, K. (2008). Pituitary homeobox 2 regulates adrenal4 binding
1052 protein/steroidogenic factor-1 gene transcription in the pituitary gonadotrope through
1053 interaction with the intronic enhancer. Mol Endocrinol *22*, 1633-1646. 10.1210/me.2007-
1054 0444.
1055 48. Shima, Y., Miyabayashi, K., Baba, T., Otake, H., Katsura, Y., Oka, S., Zubair, M., and
1056 Morohashi, K. (2012). Identification of an enhancer in the Ad4BP/SF-1 gene specific for
1057 fetal Leydig cells. Endocrinology *153*, 417-425. 10.1210/en.2011-1407.
1058 49. Menees, K.B., Earls, R.H., Chung, J., Jernigan, J., Filipov, N.M., Carpenter, J.M., and
1059 Lee, J.K. (2021). Sex- and age-dependent alterations of splenic immune cell profile and
1060 NK cell phenotypes and function in C57BL/6J mice. Immun Ageing *18*, 3.

1061 10.1186/s12979-021-00214-3.
1062 50. Czompoly, T., Labadi, A., Kellermayer, Z., Olasz, K., Arnold, H.H., and Balogh, P. (2011).
1063 Transcription factor Nkx2-3 controls the vascular identity and lymphocyte homing in the
1064 spleen. J Immunol *186*, 6981-6989. 10.4049/jimmunol.1003770.
1065 51. Lewis, S.M., Williams, A., and Eisenbarth, S.C. (2019). Structure and function of the
1066 immune system in the spleen. Sci Immunol *4*, eaau6085. 10.1126/sciimmunol.aau6085.
1067 52. Kraal, G., and Mebius, R. (2006). New insights into the cell biology of the marginal zone
1068 of the spleen. Int Rev Cytol *250*, 175-215. 10.1016/S0074-7696(06)50005-1.
1069 53. Hassanpour, M., Salybekov, A.A., Kobayashi, S., and Asahara, T. (2023). CD34 positive
1070 cells as endothelial progenitor cells in biology and medicine. Front Cell Dev Biol *11*,
1071 1128134. 10.3389/fcell.2023.1128134.
1072 54. Katoh-Fukui, Y., Owaki, A., Toyama, Y., Kusaka, M., Shinohara, Y., Maekawa, M.,
1073 Toshimori, K., and Morohashi, K. (2005). Mouse Polycomb M33 is required for splenic
1074 vascular and adrenal gland formation through regulating Ad4BP/SF1 expression. Blood
1075 *106*, 1612-1620. 10.1182/blood-2004-08-3367.
1076 55. Fatchiyah, Zubair, M., Shima, Y., Oka, S., Ishihara, S., Fukui-Katoh, Y., and Morohashi,
1077 K. (2006). Differential gene dosage effects of Ad4BP/SF-1 on target tissue development.
1078 Biochem Biophys Res Commun *341*, 1036-1045. 10.1016/j.bbrc.2006.01.058.
1079 56. Kim, S., and Wysocka, J. (2023). Deciphering the multi-scale, quantitative cis-regulatory
1080 code. Mol Cell *83*, 373-392. 10.1016/j.molcel.2022.12.032.
1081 57. Achermann, J.C., Ito, M., Ito, M., Hindmarsh, P.C., and Jameson, J.L. (1999). A mutation
1082 in the gene encoding steroidogenic factor-1 causes XY sex reversal and adrenal failure in
1083 humans. Nat Genet *22*, 125-126. 10.1038/9629.
1084 58. Camats, N., Pandey, A.V., Fernandez-Cancio, M., Andaluz, P., Janner, M., Toran, N.,
1085 Moreno, F., Bereket, A., Akcay, T., Garcia-Garcia, E., et al. (2012). Ten novel mutations
1086 in the NR5A1 gene cause disordered sex development in 46,XY and ovarian insufficiency
1087 in 46,XX individuals. J Clin Endocrinol Metab *97*, E1294-1306. 10.1210/jc.2011-3169.
1088 59. Dunn, S.E., Perry, W.A., and Klein, S.L. (2024). Mechanisms and consequences of sex
1089 differences in immune responses. Nat Rev Nephrol *20*, 37-55. 10.1038/s41581-023-
1090 00787-w.
1091 60. Bagheri-Fam, S., Combes, A.N., Ling, C.K., and Wilhelm, D. (2021). Heterozygous
1092 deletion of Sox9 in mouse mimics the gonadal sex reversal phenotype associated with
1093 campomelic dysplasia in humans. Hum Mol Genet *29*, 3781-3792. 10.1093/hmg/ddaa259.

1094 61. Bennett, J., Baumgarten, S.C., and Stocco, C. (2013). GATA4 and GATA6 silencing in
1095 ovarian granulosa cells affects levels of mRNAs involved in steroidogenesis, extracellular
1096 structure organization, IGF-I activity, and apoptosis. Endocrinology *154*, 4845-4858.
1097 10.1210/en.2013-1410.
1098

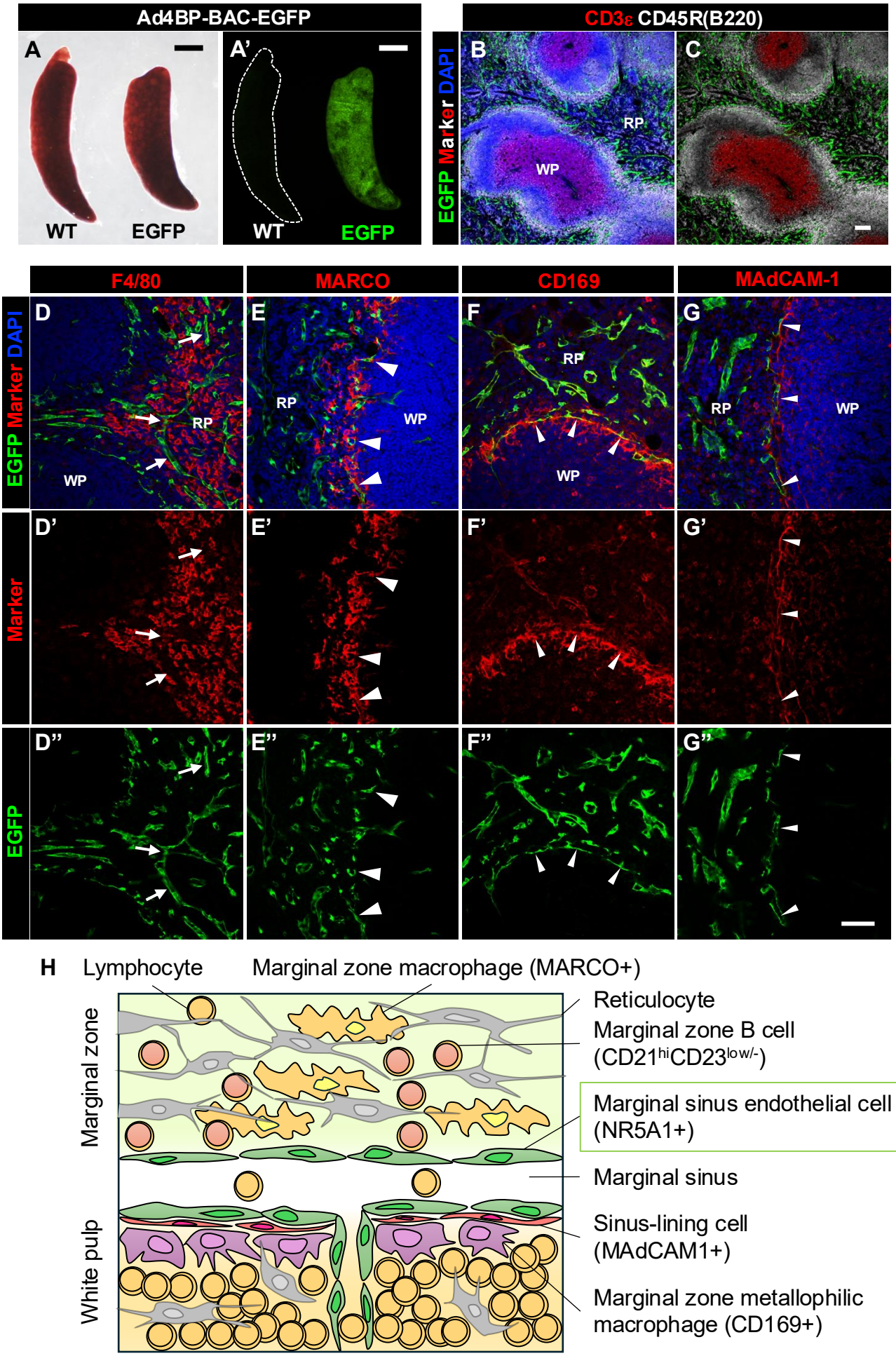

Miyabayashi, et al., Figure 1

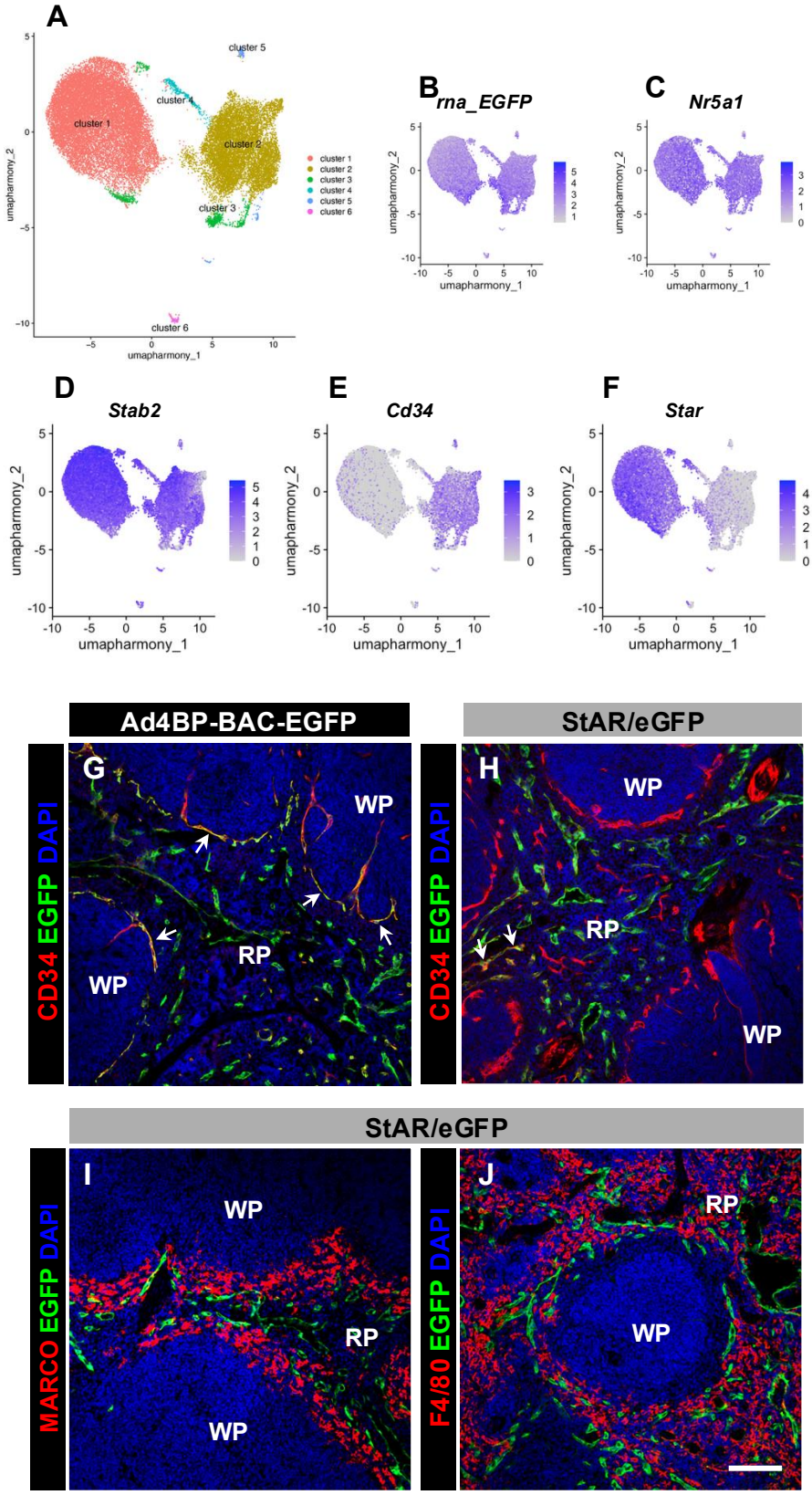

Miyabayashi, et al., Figure 2

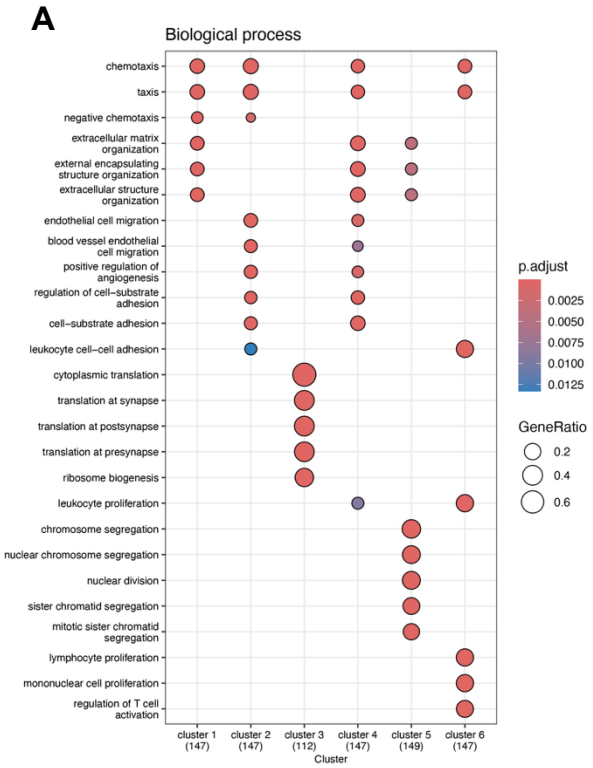

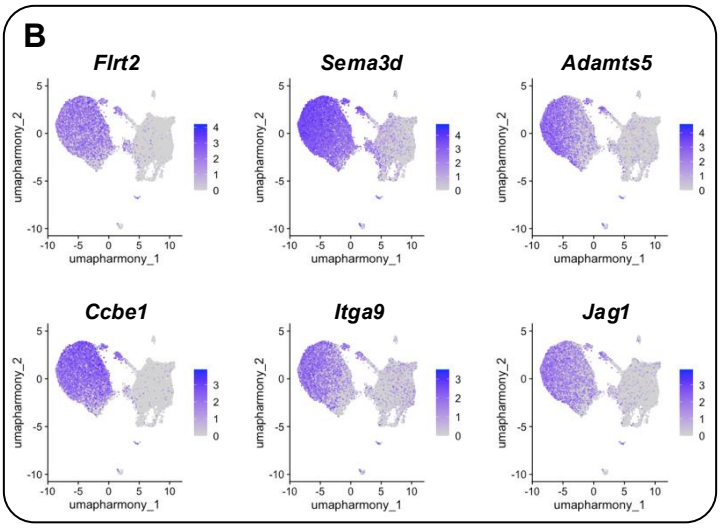

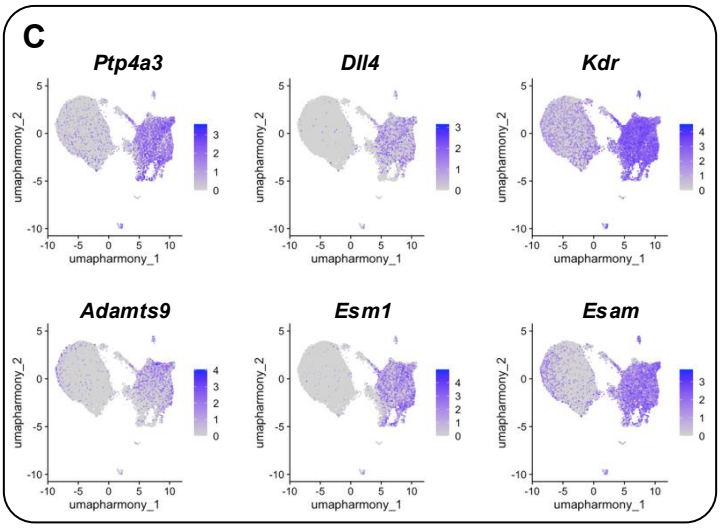

Miyabayashi, et al., Figure 3

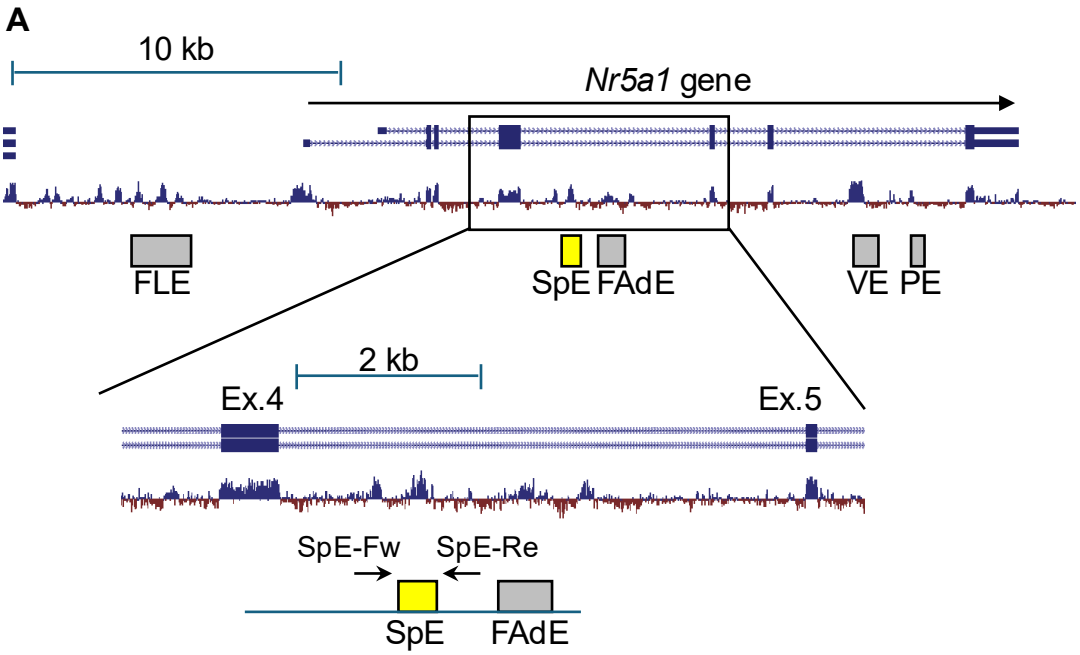

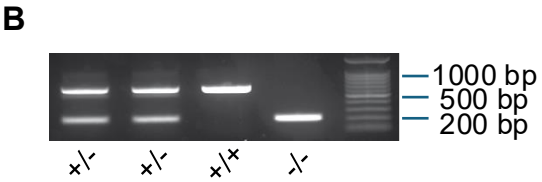

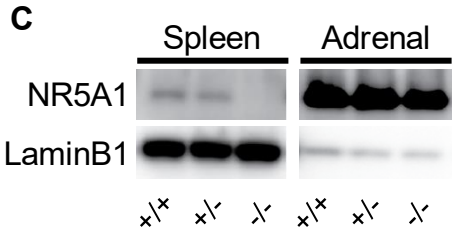

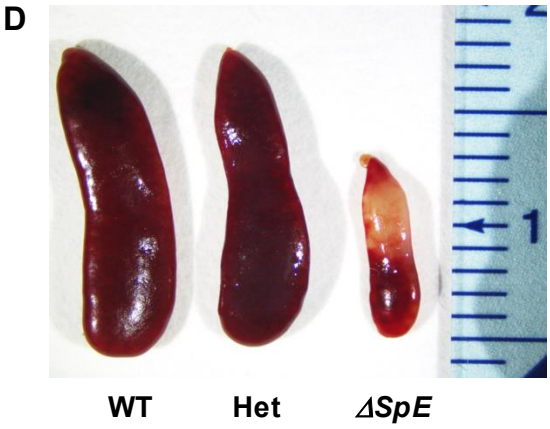

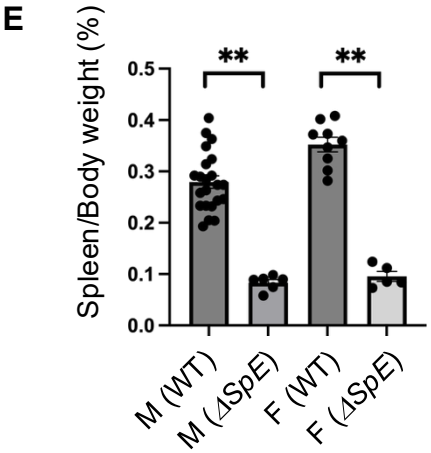

Miyabayashi, et al., Figure 4

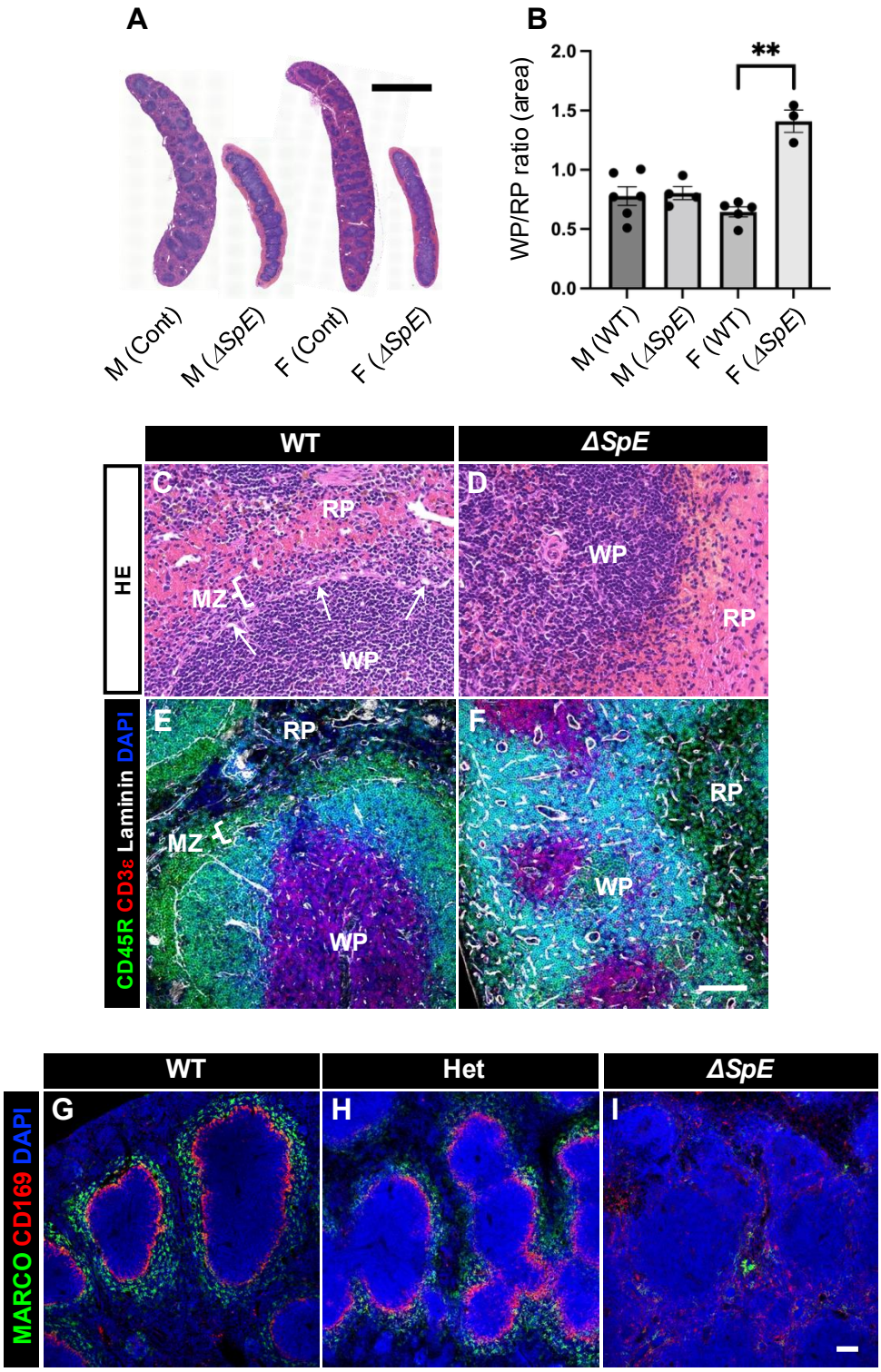

Miyabayashi, et al., Figure 5

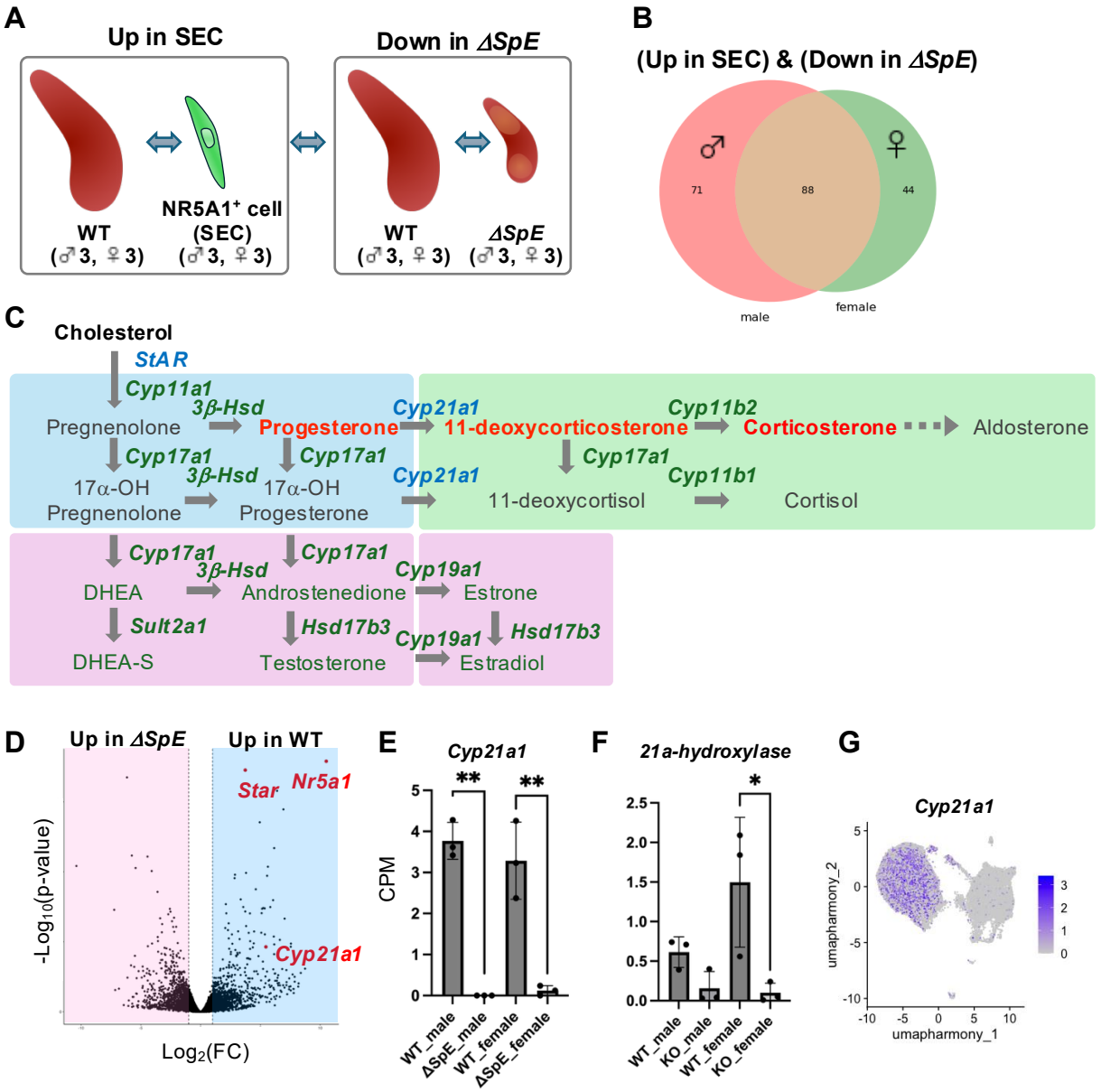

Miyabayashi, et al., Figure 6

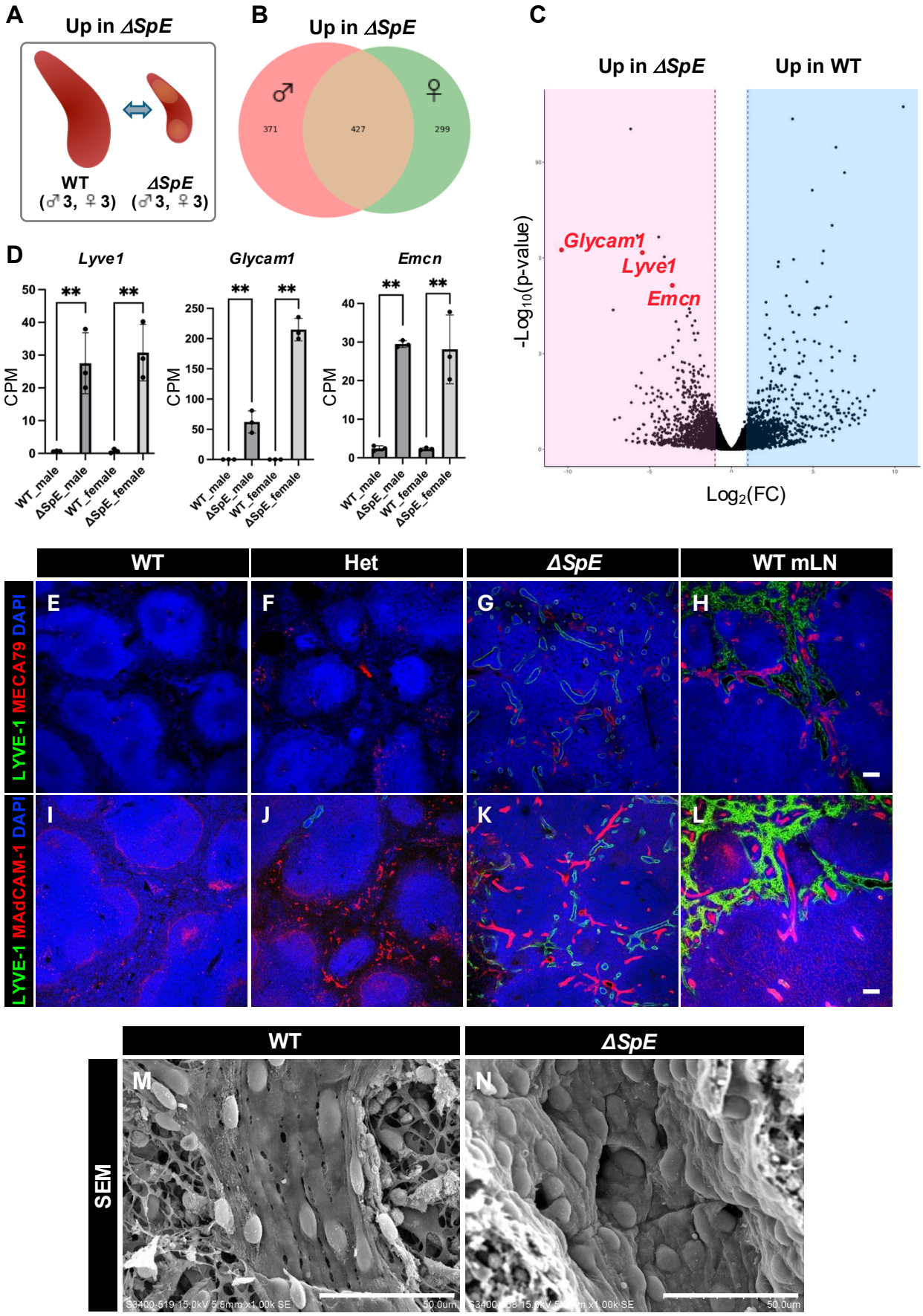

Miyabayashi, et al., Figure 7

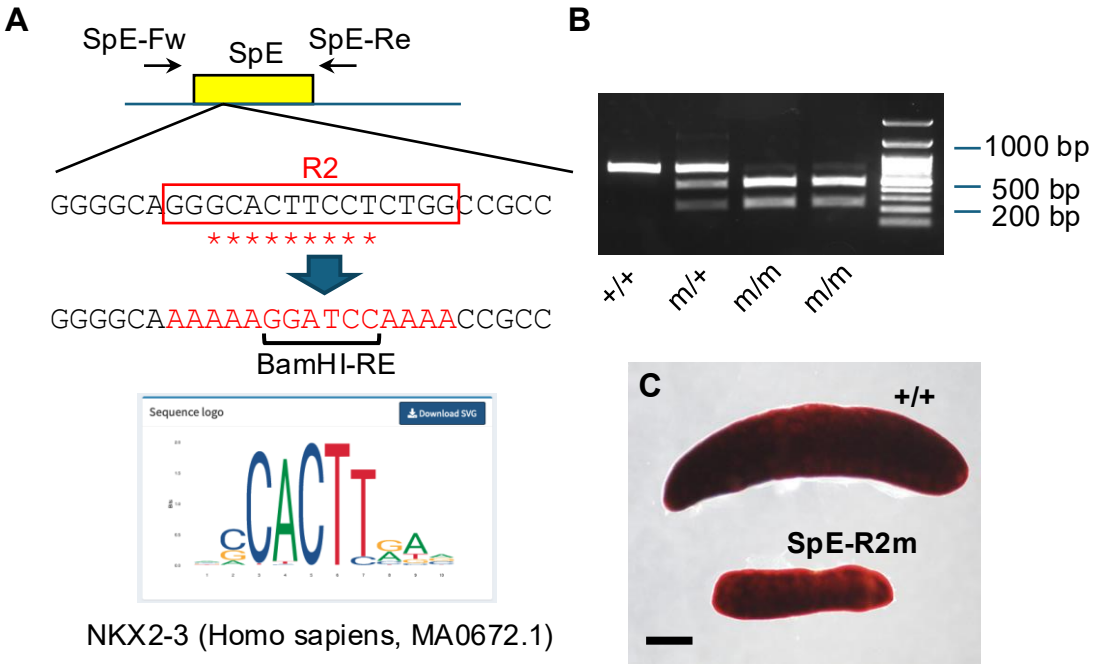

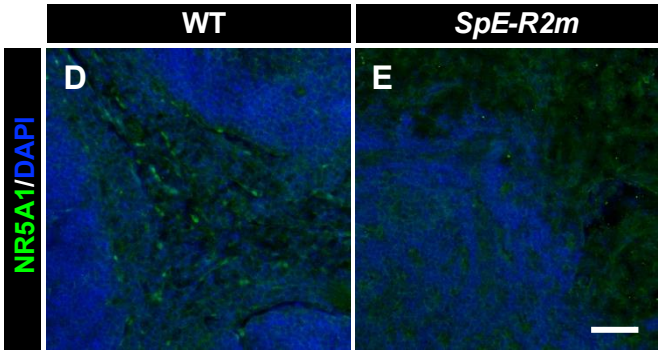

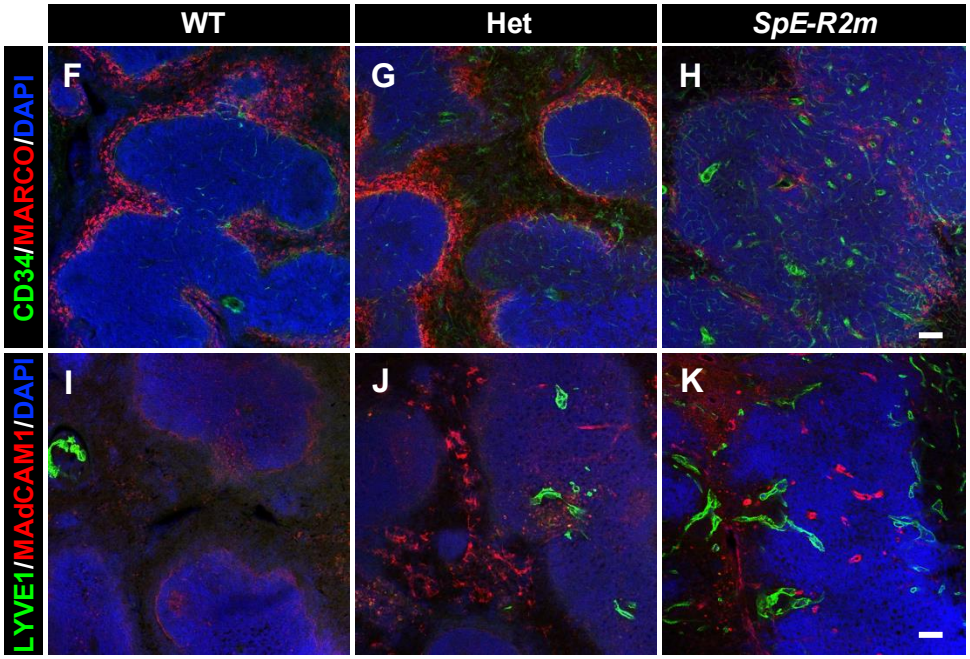

Miyabayashi, et al., Figure 8